INTERNATIONAL JOURNAL FOR NUMERICAL METHODS IN FLUIDS
Int. J. Numer. Meth. Fluids 2004; **45**:889–920 (DOI: 10.1002/fld.720)

Generalized Fourier analyses of the advection–diffusion equation—Part II: two-dimensional domains

Thomas E. Voth*,†, Mario J. Martinez and Mark A. Christon

Sandia National Laboratories, M/S 0819, P.O. Box 5800, Albuquerque, NM 87185-0819, U.S.A.

SUMMARY

Part I of this work presents a detailed multi-methods comparison of the spatial errors associated with the one-dimensional finite difference, finite element and finite volume semi-discretizations of the scalar advection–diffusion equation. In Part II we extend the analysis to two-dimensional domains and also consider the effects of wave propagation direction and grid aspect ratio on the phase speed, and the discrete and artificial diffusivities. The observed dependence of dispersive and diffusive behaviour on propagation direction makes comparison of methods more difficult relative to the one-dimensional results. For this reason, integrated (over propagation direction and wave number) error and anisotropy metrics are introduced to facilitate comparison among the various methods. With respect to these metrics, the consistent mass Galerkin and consistent mass control-volume finite element methods, and their streamline upwind derivatives, exhibit comparable accuracy, and generally out-perform their lumped mass counterparts and finite-difference based schemes. While this work can only be considered a first step in a comprehensive multi-methods analysis and comparison, it serves to identify some of the relative strengths and weaknesses of multiple numerical methods in a common mathematical framework. Published in 2004 by John Wiley & Sons, Ltd.

KEY WORDS: advection–diffusion; phase error; dispersion; discrete diffusivity; artificial viscosity

1. INTRODUCTION

In the two-dimensional analysis, the effects of grid aspect ratio, $\gamma = \Delta y/\Delta x$, and wave propagation direction, θ, on the noted numerical artifacts are examined as a function of discrete wave number. In Section 2, several metrics are introduced that provide integrated (over propagation direction and wave number) measures of anisotropy and error to allow a quantitative methods comparison. The metrics section is followed by a presentation of phase speed, discrete diffusivity, and artificial diffusivity results for the finite element, control-volume finite element, and finite difference/volume semi-discretizations in two dimensions. Finally, the results of both Parts I and II of this paper are summarized and conclusions drawn.

*Correspondence to: Thomas E. Voth, Computational Physics R&D Dept, Sandia National Laboratories, M/S 0819, P.O. Box 5800, Albuquerque, New Mexico 87185-0819.
†E-mail: tevoth@sandia.gov

Published online 4 May 2004
Received 17 April 2003
Revised 11 February 2004

2. METRICS

This paper presents the two-dimensional discrete phase speed, and discrete and artificial diffusivities for the finite difference, finite volume and finite element methods outlined in Part I of this work [1]. Relative to the one-dimensional results, the two-dimensional results add wave vector and velocity vector directions, θ and ϑ respectively (see Figure 2, Part I), to the parameter space. While the analysis methods presented in this work can generally handle the case when the advection velocity and wave vector directions are different, $\vartheta \neq \theta$, a full presentation of these results have been omitted due to practical space limitations. Instead our analyses assume $\vartheta = \theta$ to elucidate the angular sensitivity of the discrete methods, i.e. dependence on θ, significantly increases the complexity of the phase speed and diffusivity results. We relax this restriction for one selected semi-discretization to get a flavour of its effect. We recognize that group errors are also important for multi-dimensional domains, however, practical space limitations prohibit discussion of the effect here. The reader may wish to consult Gresho and Sani [2, pp. 222–234] for a additional results on two-dimensional group speed.

In order to present the two-dimensional results, polar plots are used. Figure 1 shows a plot of phase speed for a representative two-dimensional semi-discretization on a unit aspect ratio grid. In Figure 1, the radial coordinate is phase speed, $\tilde{c}/c$, and the propagation direction is associated with the azimuthal coordinate. Polar curves at fixed non-dimensional wave number are plotted in the figure with each curve representing the dimensionless phase speed for that wave number. In this work, curves at $2\Delta x/\lambda = 0$, 0.2, 0.4, 0.6, 0.8 and 1.0 are plotted. The figure clearly demonstrates the anisotropic behaviour (i.e. θ dependence) of the non-dimensional phase speed, $\tilde{c}/c$. For this example, the anisotropy becomes more pronounced as dimensionless wave number increases from 0 to 1. Note that the phase and diffusivity polar plots in this paper are constructed for the first quadrant (i.e. $0 \leqslant \theta \leqslant \pi/2$ where u and v are

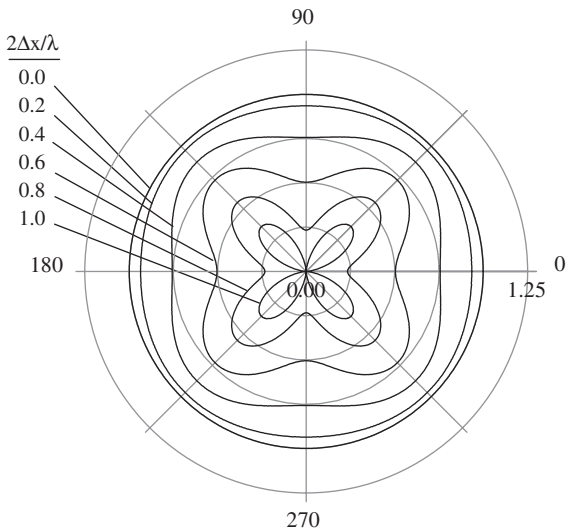

Figure 1. Non-dimensional phase speed ($\tilde{c}/c$; radial coordinate) as a function of θ (azimuthal coordinate).

positive as implied by the stencils of the Appendix, Part I) with the remaining portions being constructed by symmetry.

Although polar plots such as that shown in Figure 1 suggest the degree of anisotropy and accuracy of an individual method, a quantitative measure is desired. For this reason, two metrics are introduced. The first metric is the coefficient of variation,

$$\varsigma(2\Delta x/\lambda) = \frac{\sigma(2\Delta x/\lambda)}{\overline{G(2\Delta x/\lambda)}} \tag{1}$$

which provides a measure of the anisotropy of a method for a given dimensionless wave number. In Equation (1), G is a generic variable representing $\tilde{c}/c$ or $\tilde{\alpha}/\alpha$,

$$\overline{G(2\Delta x/\lambda)} = \frac{1}{2\pi}\int_0^{2\pi} G(2\Delta x/\lambda,\theta)\,\mathrm{d}\theta \tag{2}$$

is its mean and,

$$\sigma(2\Delta x/\lambda) = \sqrt{\frac{1}{2\pi}\int_0^{2\pi}\left(G(2\Delta x/\lambda,\theta) - \overline{G(2\Delta x/\lambda)}\right)^2\,\mathrm{d}\theta} \tag{3}$$

its standard deviation at some $2\Delta x/\lambda$.

It is clear from Equations (1)–(3) that an isotropic scheme yields $\varsigma(2\Delta x/\lambda) = 0$ because $G(2\Delta x/\lambda,\theta) = \overline{G(2\Delta x/\lambda)}$ for all θ. Similarly, large values of ς correlate to a high degree of anisotropy so that a direct comparison between methods can be made at a given wavelength, and between wavelengths for a given method. For the scheme represented by Figure 1, $\varsigma = 0.0$, 1.2×10^{-2}, 5.0×10^{-2}, 1.3×10^{-1}, 2.9×10^{-1} and 7.0×10^{-1} for $2\Delta x/\lambda = 0$, 0.2, 0.4, 0.6, 0.8 and 1.0, respectively. As indicated by $\varsigma(0)$ and suggested by the figure, the scheme is perfectly isotropic in the limit of infinite wavelength (i.e. $2\Delta x/\lambda = 0$). As wavelength decreases, the method becomes increasingly anisotropic. At the Nyquist limit, $2\Delta x/\lambda = 1$, the method demonstrates the greatest anisotropy in this measure.

The average value of the coefficient of variation,

$$\overline{\varsigma} = \int_0^1 \varsigma(2\Delta x/\lambda)\,\mathrm{d}(2\Delta x/\lambda) \tag{4}$$

is also employed here and provides a single number, independent of $2\Delta x/\lambda$, which may also be used for comparison of discretization schemes. Again, a larger value of $\overline{\varsigma}$ indicates (on average) greater anisotropy while $\overline{\varsigma} = 0$ is representative of a method that is isotropic for all wavelengths.

While the ς and $\overline{\varsigma}$ metrics provide a quantitative measure of a method's anisotropy in phase and discrete diffusivity, they do not provide a measure of the error associated with a discretization. Indeed, it is possible for a discretization scheme to have significant error in phase or diffusivity, while still demonstrating isotropic behaviour. In the case of phase speed, this (unlikely) result is characterized by a perfectly isotropic phase which differs from the ideal such that $\overline{\tilde{c}(2\Delta x/\lambda)} = \tilde{c}(2\Delta x/\lambda,\theta) \neq c$. For this reason, we introduce a second metric, the RMS error metric,

$$\varepsilon(2\Delta x/\lambda) = \sqrt{\frac{1}{2\pi}\int_0^{2\pi}(G(2\Delta x/\lambda,\theta) - g(2\Delta x/\lambda,\theta))^2\,\mathrm{d}\theta} \tag{5}$$

This metric measures the azimuthal deviation of G from its true (i.e. physical) value g. For dimensionless phase speed and discrete diffusivity, $g=1$. Hence, an ideal scheme will have $\varepsilon(2\Delta x/\lambda)=0$ for all wavelengths $0\leqslant 2\Delta x/\lambda<1$. For the scheme represented by Figure 1, $\varepsilon=0.0$, 5.0×10^{-2}, 1.9×10^{-1}, 3.9×10^{-1}, 6.2×10^{-1} and 8.3×10^{-1} for $2\Delta x/\lambda=0$, 0.2, 0.4, 0.6, 0.8 and 1.0, respectively.

The average value of ε over $2\Delta x/\lambda$,

$$\bar{\varepsilon}=\int_0^1 \varepsilon(2\Delta x/\lambda)\,\mathrm{d}(2\Delta x/\lambda) \tag{6}$$

is also employed here as it provides a single error metric that facilitates methods comparison. Larger values of $\bar{\varepsilon}$ indicate, on average, larger errors for the method. The method of Figure 1 yields $\bar{\varepsilon}=3.3\times10^{-2}$ in terms of phase speed.

3. RESULTS

3.1. Phase speed

This section begins with a presentation of the analytic expressions for the non-dimensional phase speed for all the semi-discrete methods considered. A summary of the phase speed results in terms of polar plots and the anisotropy and error metrics follows.

Phase speed formulae. Owing to the nature of the linear advection–diffusion equation, the trial solution and the Cartesian grid, the two-dimensional dispersion formulae for some of the methods can be written in terms of the one-dimensional formulae presented in Part I. The representation of the two-dimensional phase formulae in terms of the one-dimensional formulae is particularly useful in understanding the complex dispersive behaviour for the two-dimensional discretizations. Thus, the two-dimensional phase speed for FEM, CVFEM, CD, SOU, TOU, Fromm and QUICK can be written as

$$\frac{\tilde{c}}{c}=\cos^2\theta F_{\tilde{c}}^{1D}(k\Delta x\cos\theta)+\sin^2\theta F_{\tilde{c}}^{1D}(k\Delta y\sin\theta) \tag{7}$$

In Equation (7) $F_{\tilde{c}}^{1D}(\varphi)$ is the method's one-dimensional phase speed formula (cf. Table II, Part I) where $\varphi=k\Delta x$ is replaced by $k\Delta x\cos\theta$ or $k\Delta y\sin\theta$. Using consistent mass FEM as an example,

$$F_{\tilde{c}}^{1D}(\varphi)=\frac{\sin(\varphi)}{\varphi}\,\frac{3}{2+\cos(\varphi)} \tag{8}$$

and hence the phase speed formula is

$$\begin{aligned}\frac{\tilde{c}}{c}=&\cos^2\theta\frac{\sin(k\Delta x\cos\theta)}{k\Delta x\cos\theta}\,\frac{3}{2+\cos(k\Delta x\cos\theta)}\\&+\sin^2\theta\frac{\sin(\gamma k\Delta x\sin\theta)}{\gamma k\Delta x\sin\theta}\,\frac{3}{2+\cos(\gamma k\Delta x\sin\theta)}\end{aligned} \tag{9}$$

where $\gamma\Delta x = \Delta y$ has been used (cf. Equation (2.6-200) in Gresho and Sani [2]). As noted earlier, our analyses assume (for clarity) that the wave number and velocity vectors are aligned (i.e. $\theta = \vartheta$). This is not strictly necessary and we may perform a similar analysis for $\theta \neq \vartheta$. A flavour of the resulting phase speed behaviour is presented later for the consistent mass FEM. Presenting these more complicated behaviours for the other semi-discretizations considered here is beyond the scope of this work and so, again, unless otherwise noted, the remaining discussions are for $\theta = \vartheta$.

As expected, the one-dimensional formula is recovered along the co-ordinate directions (i.e. $\theta = 0, \pi/2, \pi$, and $3\pi/2$), in terms of the corresponding mesh increment (Δx or Δy) for the co-ordinate direction. Furthermore, for plane waves propagating normal to the diagonal ($\theta = \pi/4$) of a square grid ($\gamma = 1$), the two-dimensional formula reverts to the one-dimensional result, but with an effective grid spacing of $\Delta x_{\text{eff}} = \Delta x\sqrt{2}/2$,

$$\frac{\tilde{c}}{c} = \frac{\sin(k\Delta x_{\text{eff}})}{k\Delta x_{\text{eff}}} \frac{3}{2 + \cos(k\Delta x_{\text{eff}})} \tag{10}$$

In general, the two-dimensional phase speed can be written in an analogous one-dimensional form whenever $\theta = \theta^* = \arctan(1/\gamma)$. In this case $\Delta x \cos\theta = \Delta y \sin\theta$ and hence Equation (7) reduces to

$$\frac{\tilde{c}}{c} = F_{\tilde{c}}^{1D}(k\Delta x \cos\theta^*) \tag{11}$$

This is the one-dimensional phase speed on a grid with an effective spacing of $\Delta x \cos\theta^*$. In the following results section, the effect of this 'enhanced' resolution along the directions normal to the grid diagonals will be realized by a reduced phase error compared to those along the co-ordinate directions.

Remark
When considering grids with aspect ratios other than unity, the appropriate Nyquist frequency of the mesh should be based on the larger of Δx or Δy, i.e. the coarsest mesh spacing. In the ensuing discussion, only $\gamma \leqslant 1$ are considered which implies that the Nyquist limit for the grid will be based on Δx. Consideration of $\gamma > 1$ would require that the grid Nyquist limit be based on Δy.

As suggested above, several of the methods considered cannot be written in the form of Equation (7). These include the central difference with consistent mass (CD-$\mathbf{M}_c$), the LSR schemes, SUPG, and SUCV. The CD-$\mathbf{M}_c$ method is an *ad hoc* method derived by assuming linear variation of the unknown over the control volumes for the mass matrix, and using standard CD for the advection operator. Its two-dimensional phase speed is given by

$$\frac{\tilde{c}}{c} = \frac{16}{(3 + \cos\theta_x)(3 + \cos\theta_y)} \left(\cos^2\theta \frac{\sin\theta_x}{\theta_x} + \sin^2\theta \frac{\sin\theta_y}{\theta_y} \right) \tag{12}$$

where we have introduced the notation $\theta_x = k\Delta x \cos\theta$, and $\theta_y = \gamma k \Delta x \sin\theta$ $(= k\Delta y \sin\theta)$. Equation (12) cannot be cast in the general form of Equation (7) because it does not revert to the one-dimensional formula when the wave propagation direction is at right angles to the mesh diagonals.

However, as with the methods discussed above, one-dimensional behaviour is obtained for propagation angles aligned with coordinate axes. Not surprisingly, both CD-$\mathbf{M}_c$ and CVFEM yield identical phase speed behaviours along coordinate axes because their one-dimensional formulae are identical (cf. Table II of Part I). Finally, it is of interest to note that lumping the CD-$\mathbf{M}_c$ mass matrix results in the leading term on the right-hand side of Equation (12) becoming unity, and the formula reverts to the phase speed for the CD method,

$$\frac{\tilde{c}}{c} = \left(\cos^2\theta \frac{\sin\theta_x}{\theta_x} + \sin^2\theta \frac{\sin\theta_y}{\theta_y} \right) \tag{13}$$

which follows the simple form of Equation (7).

The phase speed for LSR(0) is given by

$$\begin{aligned} \frac{\tilde{c}}{c} &= \cos^2\theta \frac{1}{12\theta_x} [2\sin\theta_x(7 + 2\cos\theta_y) - \sin 2\theta_x(1 + 2\cos\theta_y)] \\ &\quad + \sin^2\theta \frac{1}{12\theta_y} [2\sin\theta_y(7 + 2\cos\theta_x) - \sin 2\theta_y(1 + 2\cos\theta_x)] \end{aligned} \tag{14}$$

This scheme also does not follow the general form of Equation (7), as it contains terms involving cross products of the x and y components. These cross-terms arise because the advection stencils include terms from all neighbouring grid points (cf. Appendix of Part I). This is also true for the FEM and CVFEM operators, however the symbol factors conveniently to eliminate the cross terms. Along the coordinate directions (i.e., in one dimension) Equation (14) becomes

$$\frac{\tilde{c}}{c} = \frac{1}{4\varphi}(6\sin\varphi - \sin 2\varphi) \tag{15}$$

where $\varphi = \theta_x$ along the x direction and $\varphi = \theta_y$ along the y direction. Incidentally, this is the one-dimensional version of Fromm's method.

The phase speed for LSR(-1) is

$$\begin{aligned} \frac{\tilde{c}}{c} &= \cos^2\theta \frac{1}{6\theta_x} [4(2 + \cos\theta_y)\sin\theta_x - (1 + 2\cos\theta_y)\sin 2\theta_x] \\ &\quad + \sin^2\theta \frac{1}{6\theta_y} [4(2 + \cos\theta_x)\sin\theta_y - (1 + 2\cos\theta_x)\sin 2\theta_y] \end{aligned} \tag{16}$$

Along the coordinate directions the phase speed is

$$\frac{\tilde{c}}{c} = \frac{1}{2\varphi}(4\sin\varphi - \sin 2\varphi) \tag{17}$$

where $\varphi = \theta_x$ along the x direction and $\varphi = \theta_y$ along the y direction. This is the one-dimensional formula for SOU.

The phase speed formulae for SUPG and SUCV are given by

$$\frac{\tilde{c}}{c} = \frac{(\cos^2\theta\mathscr{G}(\theta_x) + \sin^2\theta\mathscr{G}(\theta_y))}{[1+\beta^2(\theta_x+\theta_y)^2(\cos^2\theta\mathscr{G}(\theta_x)+\sin^2\theta\mathscr{G}(\theta_y))^2]} \times \left[1 + \frac{\beta_\theta}{2}\left(\left(\frac{1}{Pe_x} + 2\beta_\theta\cos^2\theta\right)\mathscr{F}(\theta_x) + \frac{4\cos\theta\sin\theta}{\gamma}\beta_\theta\mathscr{G}(\theta_x)\mathscr{G}(\theta_y) + \left(\frac{1}{Pe_y} + 2\beta_\theta\sin^2\theta\right)\mathscr{F}(\theta_y)\right)\right] \tag{18}$$

where

$$\mathscr{F}(\varphi) = \frac{2(1-\cos\varphi)}{\mathscr{M}(\varphi)}$$
$$\mathscr{G}(\varphi) = \frac{\sin\varphi}{\varphi}\frac{1}{\mathscr{M}(\varphi)}$$
$$\beta_\theta = \beta(\cos\theta + \gamma\sin\theta) \tag{19}$$
$$Pe_x = \frac{c\Delta x}{2\alpha}, \quad Pe_y = \frac{c\Delta y}{2\alpha}$$

$\mathscr{M}(\varphi)$ is the symbol for the mass matrix operator given in Table I of Part I and β is the stabilization parameter. The two-dimensional formula reverts to the one-dimensional formula along the coordinate directions.

Phase speed results. The phase speed results for our two-dimensional semi-discretizations are presented in Figures 2–15. Figures (a) and (b) for each semi-discretization present $\tilde{c}/c$ for

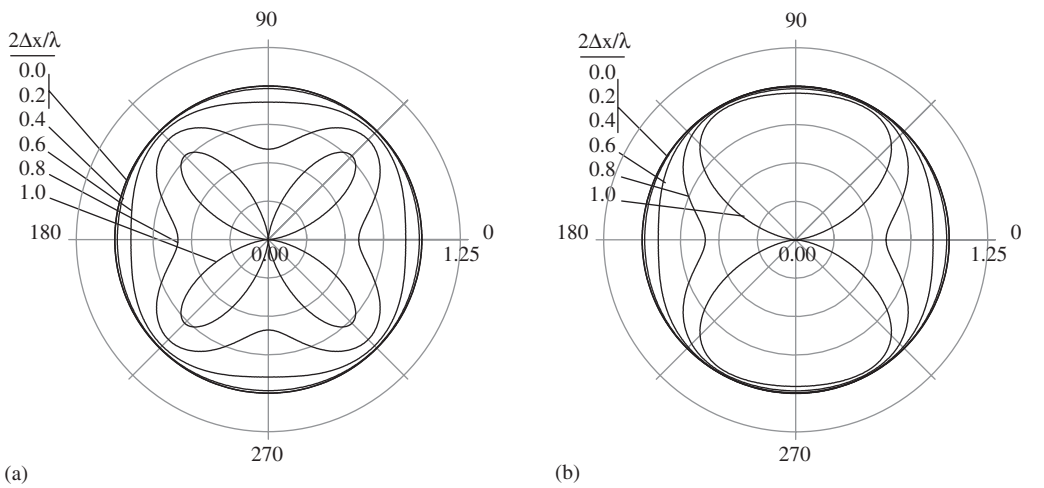

Figure 2. Non-dimensional phase speed ($\tilde{c}/c$; radial) as a function of θ (azimuthal) for the consistent mass Galerkin finite element method (FEM-$\mathbf{M}_c$) with (a) $\gamma = 1$ and (b) $\gamma = \frac{1}{2}$.

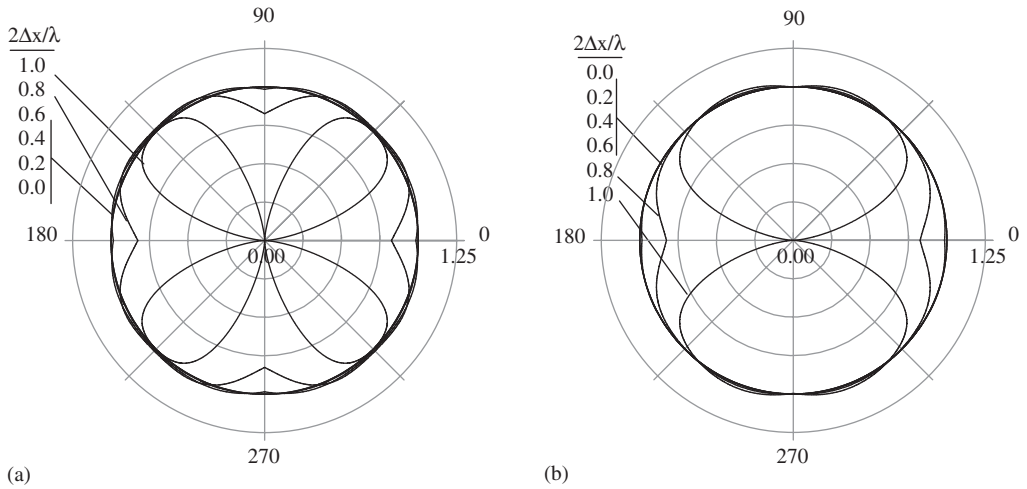

Figure 3. Non-dimensional phase speed ($\tilde{c}/c$; radial) as a function of θ (azimuthal) for consistent mass matrix finite element method SUPG with β_{opt}; (a) $\gamma = 1$ and (b) $\gamma = \frac{1}{2}$.

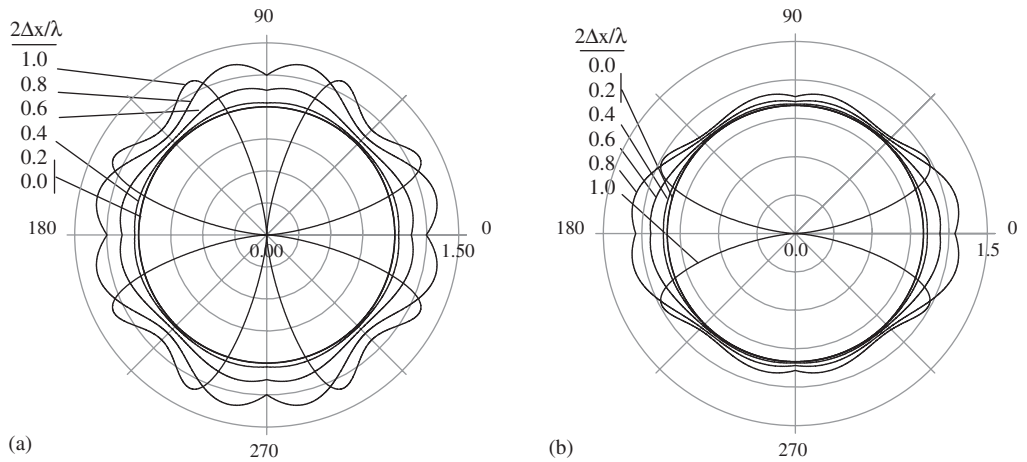

Figure 4. Non-dimensional phase speed ($\tilde{c}/c$; radial) as a function of θ (azimuthal) for consistent mass matrix finite element method SUPG with $\beta = \frac{1}{2}$; (a) $\gamma = 1$ and (b) $\gamma = \frac{1}{2}$.

grid aspect ratios of $\gamma = 1$ and $\frac{1}{2}$, respectively. As in the example polar plot, Figure 1, phase speed curves are plotted for $2\tilde{\Delta}x/\lambda = 0$, 0.2, 0.4, 0.6, 0.8 and 1.0. In the absence of phase errors, the ideal semi-discrete phase speed would exactly replicate the continuous phase speed for the entire discrete spectrum from the limit $2\Delta x/\lambda \to 0$ to the grid Nyquist limit. Hence, in the ideal case, the phase speed curves would be circular, each giving $\tilde{c}/c = 1$. However, all of the methods considered here introduce either leading or lagging phase speeds, the magnitudes of which are dependent on wavelength, grid aspect ratio and propagation direction.

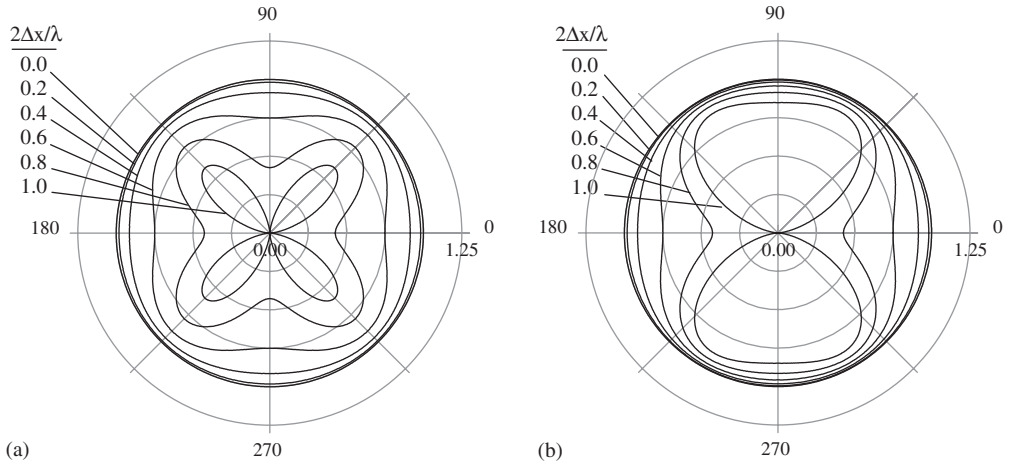

Figure 5. Non-dimensional phase speed ($\tilde{c}/c$; radial) as a function of θ (azimuthal) for the consistent mass control volume finite element method (CVFEM) with (a) $\gamma = 1$ and (b) $\gamma = \frac{1}{2}$.

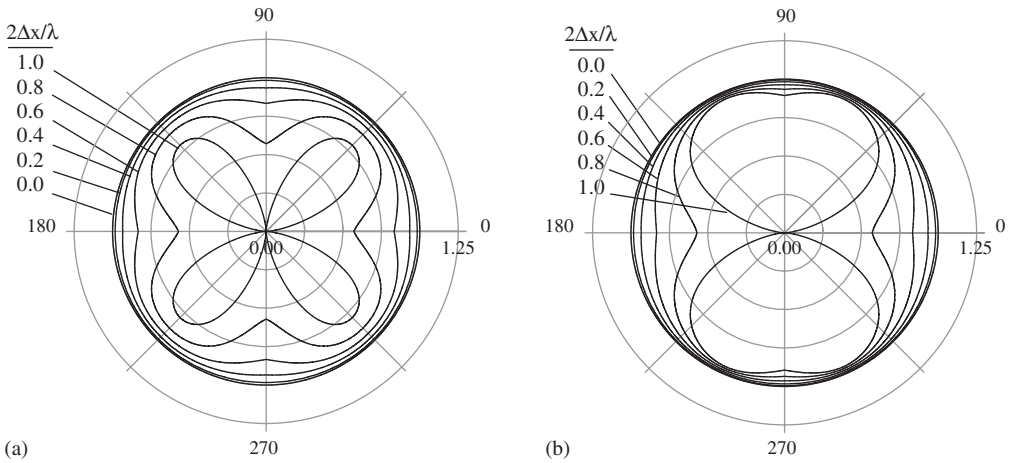

Figure 6. Non-dimensional phase speed ($\tilde{c}/c$; radial) as a function of θ (azimuthal) for consistent mass matrix control volume finite element method SUCV with β_{opt}; (a) $\gamma = 1$ and (b) $\gamma = \frac{1}{2}$.

Several points regarding the semi-discretizations are noted before beginning the discussion of results. First, phase speed for the FEM-SUPG (Figures 3 and 4) and CVFEM-SUCV (Figures 6 and 7) are presented for pure advection, i.e. when $\mathbf{P}_e \to \infty$. Second, results for the lumped mass variants of FEM and CVFEM are not included here as their results are significantly degraded relative to their consistent mass counterparts (see Part I for examples of the effects of mass lumping). Finally, the reader is reminded that the FOU scheme may be decomposed into a centred second-order advection scheme with concomitant second-order centred diffusion operator. For this reason, phase speed results for the FOU and CD scheme are identical and so presented as one result.

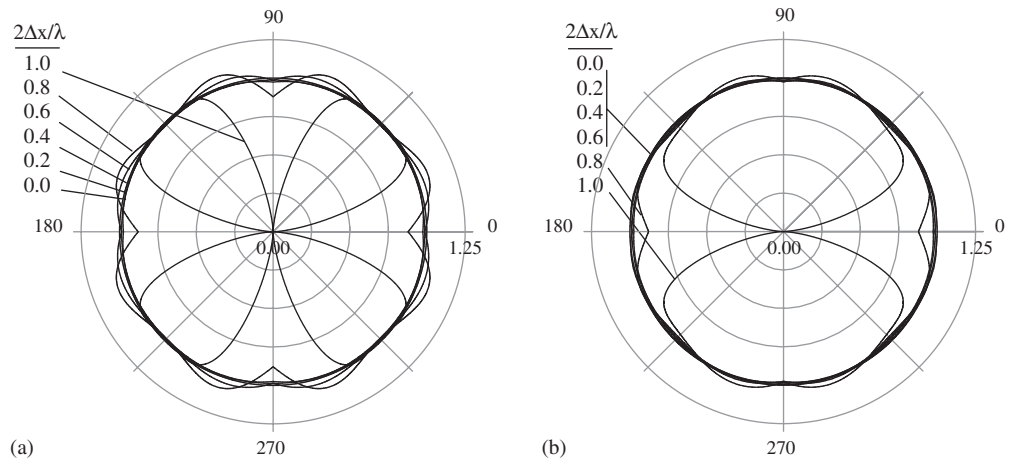

Figure 7. Non-dimensional phase speed ($\tilde{c}/c$; radial) as a function of θ (azimuthal) for consistent mass matrix control volume finite element method SUCV with $\beta = \frac{1}{2}$; (a) $\gamma = 1$ and (b) $\gamma = \frac{1}{2}$.

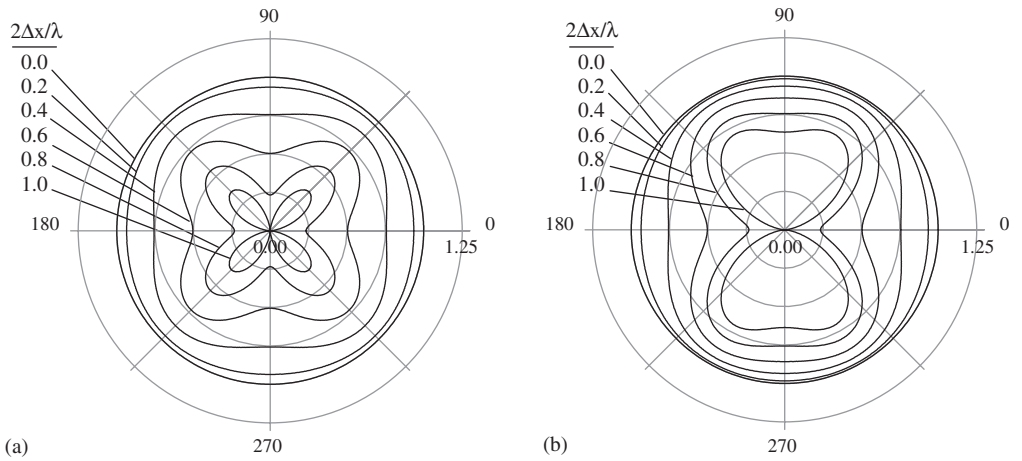

Figure 8. Non-dimensional phase speed ($\tilde{c}/c$; radial) as a function of θ (azimuthal) for the central difference method (also FOU). Results for aspect ratios of (a) $\gamma = 1$ and (b) $\gamma = \frac{1}{2}$ are shown.

Several characteristics are evident from the series of figures presented here. First, the figures clearly indicate anisotropic wave propagation for all schemes considered with the $\gamma = \frac{1}{2}$ cases demonstrating less θ-dependence than their $\gamma = 1$ counterparts. Indeed, the $\gamma = 1$ cases all show quarter-symmetry while the $\gamma = \frac{1}{2}$ discretizations show half-symmetry, both behaviours being consistent with the symmetry of their respective spatial grids. It is also evident from the figures that this anisotropy generally increases with increasing $2\Delta x/\lambda$. This observation is demonstrated quantitatively in Tables I and II where the coefficient of variation of the phase speed, $\varsigma_{\tilde{c}}$, and its mean $\overline{\varsigma_{\tilde{c}}}$ are presented. The tables show that $\varsigma_{\tilde{c}}$ generally grows with

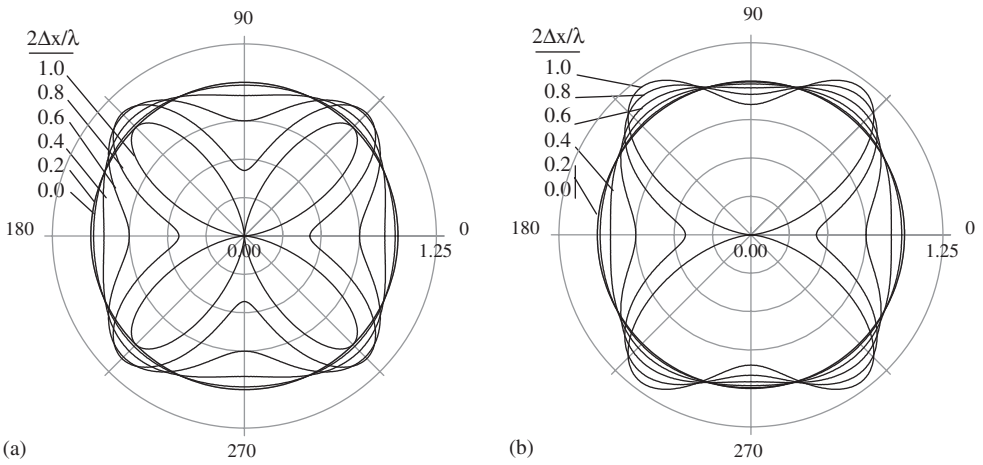

Figure 9. Non-dimensional phase speed ($\tilde{c}/c$; radial) as a function of θ (azimuthal) for the consistent mass matrix central difference discretization (CD-$\mathbf{M}_c$). Results for aspect ratios of (a) $\gamma = 1$ and (b) $\gamma = \frac{1}{2}$ are shown.

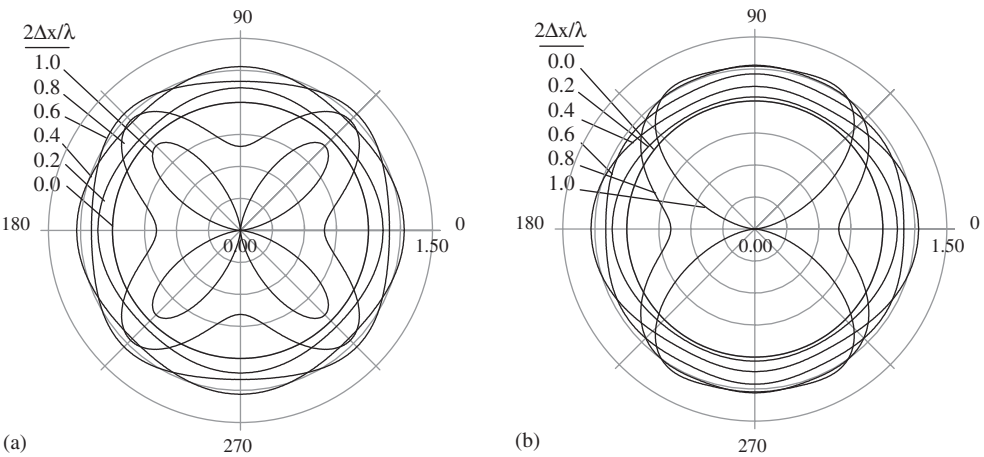

Figure 10. Non-dimensional phase speed ($\tilde{c}/c$; radial) as a function of θ (azimuthal) for the second-order upwind finite difference discretization (SOU). Results are shown for aspect ratios of (a) $\gamma = 1$ and (b) $\gamma = \frac{1}{2}$.

increasing $2\Delta x/\lambda$. In terms of the $\overline{\varsigma_{\tilde{c}}}$ metric, and relative to the grid aspect ratio, $\gamma = \frac{1}{2}$ minimizes θ-dependence for all but the LSR semi-discretizations. Finally, it is evident from a method-to-method comparison of $\overline{\varsigma_{\tilde{c}}}$ that FEM-SUPG and CVFEM-SUCV minimize anisotropic behaviour irrespective of grid aspect ratio given the proper choice of stabilization parameter. Note that the LSR schemes provide good isotropy for the $\gamma = 1$ case but become more anisotropic (relative to the other methods) for $\gamma = \frac{1}{2}$.

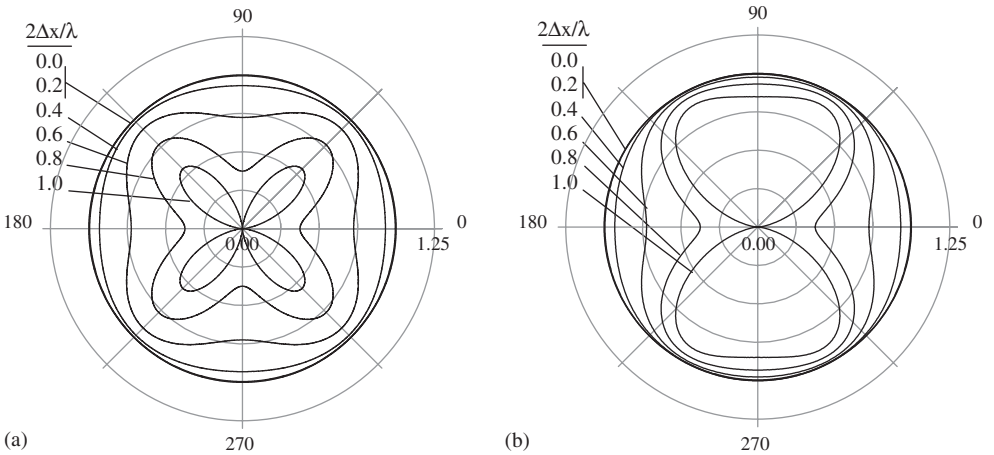

Figure 11. Non-dimensional phase speed ($\tilde{c}/c$; radial) as a function of θ (azimuthal) for the finite difference discretization with third-order-upwind (TOU) differencing. Results for aspect ratios of (a) $\gamma = 1$ and (b) $\gamma = \frac{1}{2}$ are shown.

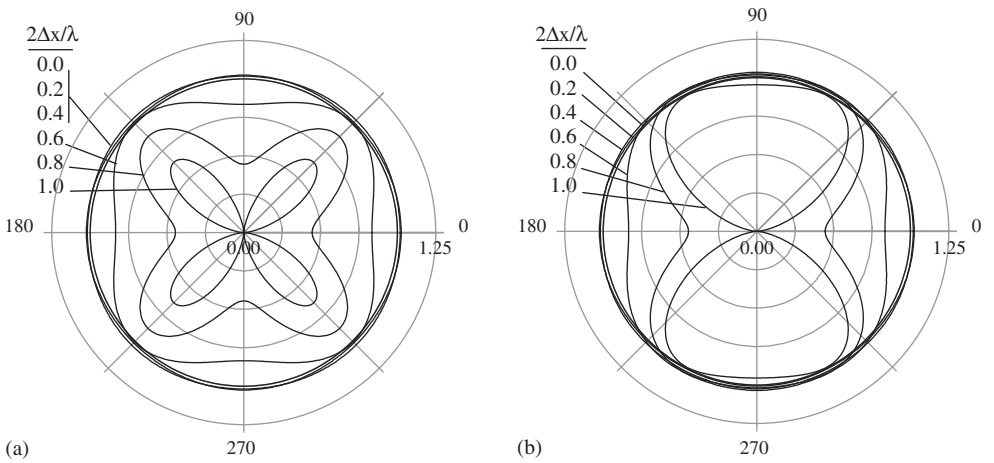

Figure 12. Non-dimensional phase speed ($\tilde{c}/c$; radial) as a function of θ (azimuthal) for Fromm's method. Results for (a) $\gamma = 1$ and (b) $\gamma = \frac{1}{2}$ are shown.

The series of figures in this section also provides information concerning the phase error of each method. As suggested by the anisotropy discussion above, this error is dependent on wave number as well as propagation angle. Indeed the methods generally demonstrate a minimum error along the $\theta = \pi/4$ and $\pi/2$ directions for the unit and $\frac{1}{2}$ aspect ratio cases respectively. These 'preferential' directions are a result of the better resolving power of the grid in these directions (cf. Section 3.1 Equation (11)). A quantitative measure of the discrete phase errors is presented in Tables III and IV. As with $\varsigma_{\tilde{c}}$, the phase errors, $\varepsilon_{\tilde{c}}$, generally

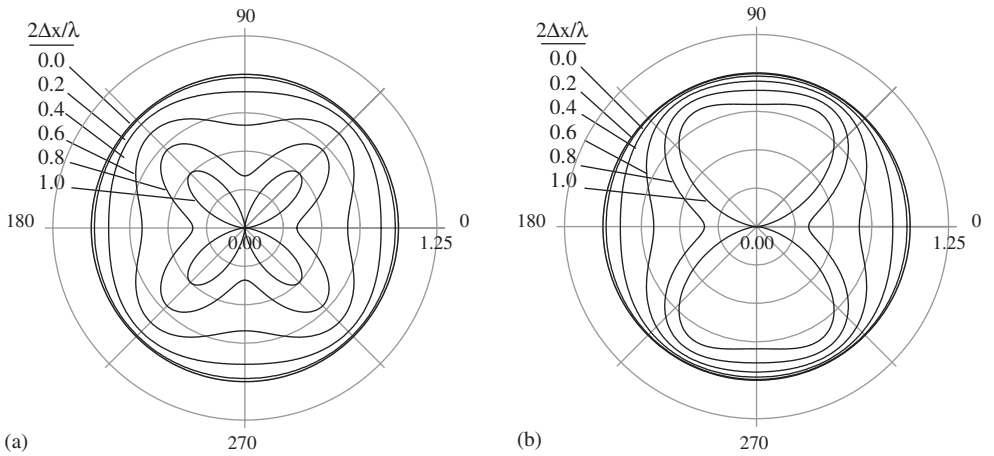

Figure 13. Non-dimensional phase speed ($\tilde{c}/c$; radial) as a function of θ (azimuthal) for the QUICK scheme with (a) $\gamma = 1$ and (b) $\gamma = \frac{1}{2}$.

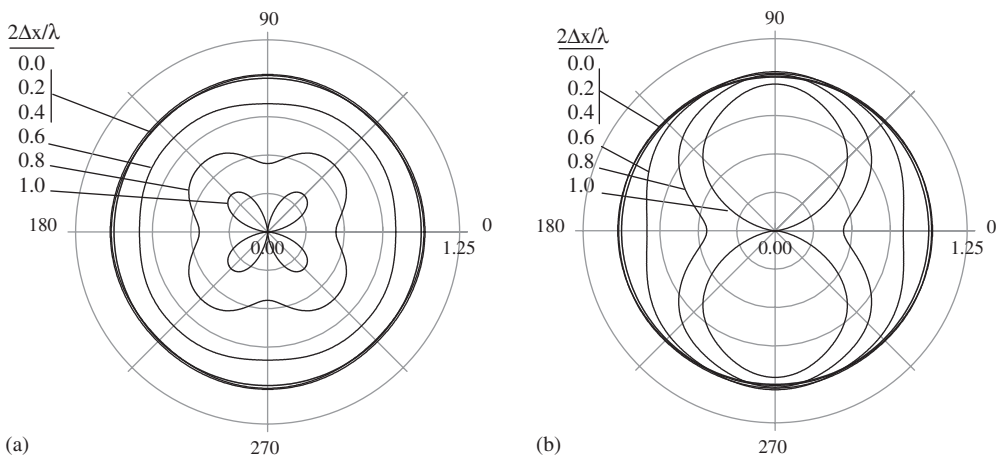

Figure 14. Non-dimensional phase speed ($\tilde{c}/c$; radial) as a function of θ (azimuthal) for the node-centered finite volume method with least squares gradient reconstruction, LSR(0), with (a) $\gamma = 1$ and (b) $\gamma = \frac{1}{2}$.

increase with increasing $2\Delta x/\lambda$, peaking at the Nyquist limit. In terms of the $\overline{\varepsilon_{\tilde{c}}}$ metric, the $\gamma = \frac{1}{2}$ results minimize phase errors relative to the unit aspect ratio cases. Finally, it is evident from a comparison of $\overline{\varepsilon_{\tilde{c}}}$ between methods, that FEM-SUPG and CVFEM-SUCV minimize errors, for either γ, given the proper choice of stabilization parameter ($\beta = \beta_{\text{opt}}$ and $\frac{1}{2}$ for SUPG and SUCV, respectively). Note that FOU demonstrates by far the worst phase error (in terms of $\overline{\varepsilon_{\tilde{c}}}$) relative to the other semi-discretizations, regardless of aspect ratio.

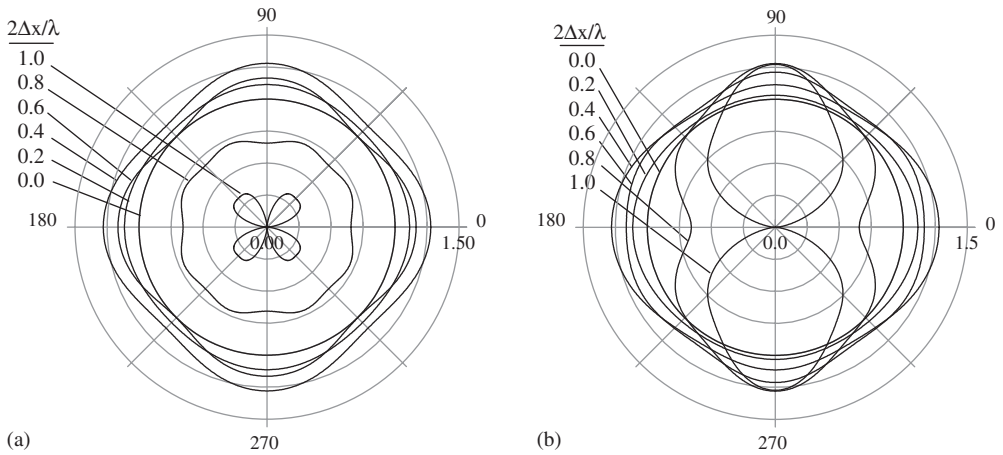

Figure 15. Non-dimensional phase speed ($\tilde{c}/c$; radial) as a function of θ (azimuthal) for the node-centered finite volume method with least squares gradient reconstruction, LSR(-1), with (a) $\gamma = 1$ and (b) $\gamma = \frac{1}{2}$.

Phase speed results for $\vartheta \neq \theta$. Although the bulk of our analyses assume that the wave and velocity vectors are aligned, here we relax this restriction in order to show the effects on the phase velocity. Specifically, we consider the consistent mass Galerkin finite element semi-discretization (FEM-$\mathbf{M}_c$). The resulting equation for the discrete phase speed is given by

$$\begin{aligned} \tilde{c}/\|\mathbf{u}\| = {} & [\cos\vartheta\cos\theta(\sin\theta_x/\theta_x)(3/(2+\cos\theta_x)) \\ & + \sin\vartheta\sin\theta(\sin\theta_y/\theta_y)(3/(2+\cos\theta_y))] \end{aligned} \tag{20}$$

where we have normalized the discrete phase speed by the magnitude of the advective velocity rather than the continuous phase speed,

$$c/\|\mathbf{u}\| = \mathbf{u}\cdot\mathbf{k}/k\|\mathbf{u}\| = [\cos\vartheta\cos\theta + \sin\vartheta\sin\theta] \tag{21}$$

as is done for the $\theta = \vartheta$ cases (cf. Equation (2.6-200) in Gresho and Sani [2]). We chose this normalization here as the normalization $\tilde{c}/c$ used elsewhere is generally unbounded (Equation (21) has zero-crossings when Equation (20) is finite) for the $\theta \neq \vartheta$ cases.

Figure 16 (a) and (b) illustrate the non-dimensional discrete phase speed, Equation (20), for wave vector angles $\theta = \pi/8,\ \pi/4$, respectively at dimensionless wave numbers of $2\Delta x/\lambda = 0$, 0.2, 0.4, 0.6, 0.8, 1.0. In the figures, the azimuthal co-ordinate represents the direction of the velocity vector, ϑ. Results are presented for $\gamma = 1$ and positive and negative values are shown as solid and dashed lines, respectively. The continuous non-dimensional phase speed of Equation (21) is also presented in the figure as the bold solid/dashed lines and represents the ideal. Several points are evident from the figures. First, the continuous phase speed forms lobes that exhibit quarter symmetry about $\theta + n\pi/2$ and are independent of wave number. The

Table I. Coefficient of variation of phase speed, $\varsigma_{\tilde{c}}$, as a function of $2\Delta x/\lambda$, and its average, $\overline{\varsigma_{\tilde{c}}}$, for the two-dimensional, $\gamma = 1$ semi-discretizations.

	$\varsigma_{\tilde{c}}$ as a function of $2\Delta x/\lambda$						
Method	0.0	0.2	0.4	0.6	0.8	1.0	$\overline{\varsigma_{\tilde{c}}}$
FEM-$\mathbf{M}_c$	0.0	2.43e − 4	4.60e − 3	3.14e − 2	1.55e − 1	7.45e − 1	1.13e − 1
SUPG β_{opt}	0.0	9.36e − 5	1.48e − 3	8.64e − 3	6.44e − 2	6.43e − 1	7.92e − 2
SUPG $\beta = \frac{1}{2}$	0.0	6.13e − 4	8.79e − 3	3.68e − 2	7.56e − 2	5.32e − 1	7.75e − 2
CVFEM-$\mathbf{M}_c$	0.0	3.26e − 3	1.79e − 2	6.48e − 2	2.11e − 1	7.40e − 1	1.33e − 1
SUCV β_{opt}	0.0	2.95e − 3	1.27e − 2	3.82e − 2	1.41e − 1	6.80e − 1	1.07e − 1
SUCV $\beta = \frac{1}{2}$	0.0	2.17e − 3	4.37e − 3	1.77e − 2	4.92e − 2	5.81e − 1	7.28e − 2
FOU/CD	0.0	1.19e − 2	5.06e − 2	1.29e − 1	2.85e − 1	7.00e − 1	1.65e − 1
CD-$\mathbf{M}_c$	0.0	1.19e − 2	5.21e − 2	1.38e − 1	3.22e − 1	7.60e − 1	1.81e − 1
SOU	0.0	1.72e − 2	2.39e − 2	3.53e − 2	2.15e − 1	7.72e − 1	1.36e − 1
TOU	0.0	1.31e − 3	1.85e − 2	8.22e − 2	2.47e − 1	7.38e − 1	1.44e − 1
Fromm's	0.0	3.62e − 3	5.71e − 3	6.66e − 2	2.36e − 1	7.50e − 1	1.37e − 1
QUICK	0.0	3.86e − 3	2.56e − 2	9.16e − 2	2.55e − 1	7.31e − 1	1.48e − 1
LSR(0)	0.0	4.68e − 3	8.14e − 3	1.31e − 2	1.12e − 1	6.36e − 1	9.13e − 2
LSR(−1)	0.0	1.92e − 2	4.81e − 2	5.29e − 2	2.46e − 2	5.86e − 1	8.75e − 2

Table II. Coefficient of variation of phase speed, $\varsigma_{\tilde{c}}$, as a function of $2\Delta x/\lambda$, and its average, $\overline{\varsigma_{\tilde{c}}}$, for the two-dimensional, $\gamma = \frac{1}{2}$ semi-discretizations.

	$\varsigma_{\tilde{c}}$ as a function of $2\Delta x/\lambda$						
Method	0.0	0.2	0.4	0.6	0.8	1.0	$\overline{\varsigma_{\tilde{c}}}$
FEM-$\mathbf{M}_c$	0.0	3.11e − 4	5.75e − 3	3.72e − 2	1.63e − 1	5.30e − 1	9.42e − 2
SUPG β_{opt}	0.0	3.65e − 5	4.90e − 4	3.81e − 3	5.37e − 2	4.44e − 1	5.61e − 2
SUPG $\beta = \frac{1}{2}$	0.0	8.44e − 4	1.12e − 2	4.43e − 2	8.85e − 2	3.55e − 1	6.45e − 2
CVFEM-$\mathbf{M}_c$	0.0	5.17e − 3	2.65e − 2	8.64e − 2	2.37e − 1	5.51e − 1	1.26e − 1
SUCV β_{opt}	0.0	4.68e − 3	1.89e − 2	5.03e − 2	1.51e − 1	4.91e − 1	9.40e − 2
SUCV $\beta = \frac{1}{2}$	0.0	3.50e − 3	4.67e − 3	8.47e − 3	2.83e − 2	4.04e − 1	4.94e − 2
FOU/CD	0.0	1.91e − 2	7.79e − 2	1.82e − 1	3.39e − 1	5.62e − 1	1.80e − 1
CD-$\mathbf{M}_c$	0.0	8.82e − 3	3.99e − 2	1.11e − 1	2.60e − 1	5.22e − 1	1.36e − 1
SOU	0.0	3.02e − 2	5.80e − 2	1.23e − 2	2.07e − 1	5.71e − 1	1.18e − 1
TOU	0.0	1.70e − 3	2.41e − 2	1.04e − 1	2.76e − 1	5.65e − 1	1.38e − 1
Fromm's	0.0	6.62e − 3	2.17e − 3	7.38e − 2	2.54e − 1	5.67e − 1	1.24e − 1
QUICK	0.0	5.94e − 3	3.65e − 2	1.21e − 1	2.90e − 1	5.65e − 1	1.47e − 1
LSR(0)	0.0	6.73e − 3	3.49e − 3	6.80e − 2	2.44e − 1	5.75e − 1	1.22e − 1
LSR(−1)	0.0	3.04e − 2	6.17e − 2	2.71e − 2	1.92e − 1	5.95e − 1	1.22e − 1

discrete phase speeds exhibit a similar symmetry for the $\theta = \pi/4$ case but deviate from this symmetry for the $\theta = \pi/8$ case for all but the very small wave number (long wavelength) signals. Interestingly, quarter symmetry appears to be generally preserved for the discrete phase (for $\theta = \pi/8$), but with symmetry angles increasingly modified from the continuous

Table III. RMS error of discrete phase speed, $\varepsilon_{\tilde{c}}$, as a function of $2\Delta x/\lambda$, and its average, $\overline{\varepsilon_{\tilde{c}}}$, for the two-dimensional, $\gamma = \frac{1}{2}$ semi-discretizations.

	$\varepsilon_{\tilde{c}}$ as a function of $2\Delta x/\lambda$						
Method	0.0	0.2	0.4	0.6	0.8	1.0	$\overline{\varepsilon_{\tilde{c}}}$
FEM-$\mathbf{M}_c$	0.0	6.14e − 4	1.12e − 2	6.92e − 2	2.71e − 1	6.90e − 1	1.39e − 1
SUPG β_{opt}	0.0	2.81e − 4	3.97e − 3	1.46e − 2	6.78e − 2	5.61e − 1	7.34e − 2
SUPG $\beta = \frac{1}{2}$	0.0	2.32e − 3	2.91e − 2	1.14e − 1	2.62e − 1	4.87e − 1	1.30e − 1
CVFEM-$\mathbf{M}_c$	0.0	1.35e − 2	6.36e − 2	1.82e − 1	4.15e − 1	7.45e − 1	2.09e − 1
SUCV β_{opt}	0.0	1.22e − 2	4.54e − 2	1.04e − 1	2.54e − 1	6.43e − 1	1.47e − 1
SUCV $\beta = \frac{1}{2}$	0.0	9.26e − 3	1.28e − 2	2.18e − 2	5.21e − 2	5.14e − 1	7.06e − 2
FOU/CD	0.0	4.99e − 2	1.89e − 1	3.91e − 1	6.17e − 1	8.29e − 1	3.32e − 1
CD-$\mathbf{M}_c$	0.0	1.20e − 2	5.30e − 2	1.46e − 1	3.39e − 1	6.41e − 1	1.74e − 1
SOU	0.0	8.97e − 2	2.39e − 1	2.25e − 1	2.14e − 1	6.60e − 1	2.20e − 1
TOU	0.0	3.38e − 3	4.75e − 2	1.94e − 1	4.55e − 1	7.61e − 1	2.16e − 1
Fromm's	0.0	1.99e − 2	2.69e − 2	1.02e − 1	3.78e − 1	7.31e − 1	1.78e − 1
QUICK	0.0	1.50e − 2	8.27e − 2	2.43e − 1	4.94e − 1	7.77e − 1	2.44e − 1
LSR(0)	0.0	1.87e − 2	1.08e − 2	1.47e − 1	4.63e − 1	8.19e − 1	2.10e − 1
LSR(−1)	0.0	8.73e − 2	2.07e − 1	1.07e − 1	3.11e − 1	8.10e − 1	2.23e − 1

Table IV. RMS error of discrete phase speed, $\varepsilon_{\tilde{c}}$, as a function of $2\Delta x/\lambda$, and its average, $\overline{\varepsilon_{\tilde{c}}}$, for the two-dimensional, $\gamma = \frac{1}{2}$ semi-discretizations.

	$\varepsilon_{\tilde{c}}$ as a function of $2\Delta x/\lambda$						
Method	0.0	0.2	0.4	0.6	0.8	1.0	$\overline{\varepsilon_{\tilde{c}}}$
FEM-$\mathbf{M}_c$	0.0	4.31e − 4	7.86e − 3	4.87e − 2	1.91e − 1	4.85e − 1	9.80e − 2
SUPG β_{opt}	0.0	7.35e − 5	9.49e − 4	3.95e − 3	5.87e − 2	4.11e − 1	5.39e − 2
SUPG $\beta = \frac{1}{2}$	0.0	1.28e − 3	1.71e − 2	6.94e − 2	1.52e − 1	3.39e − 1	8.19e − 2
CVFEM-$\mathbf{M}_c$	0.0	9.58e − 3	4.51e − 2	1.29e − 1	2.92e − 1	5.24e − 1	1.48e − 1
SUCV β_{opt}	0.0	8.88e − 3	3.45e − 2	8.23e − 2	1.97e − 1	4.66e − 1	1.11e − 1
SUCV $\beta = \frac{1}{2}$	0.0	7.17e − 3	1.42e − 2	1.24e − 2	3.34e − 2	3.80e − 1	5.15e − 2
FOU/CD	0.0	3.56e − 2	1.36e − 1	2.81e − 1	4.46e − 1	6.05e − 1	2.40e − 1
CD-$\mathbf{M}_c$	0.0	8.83e − 3	4.01e − 2	1.12e − 1	2.55e − 1	4.64e − 1	1.30e − 1
SOU	0.0	6.43e − 2	1.76e − 1	1.95e − 1	2.35e − 1	5.07e − 1	1.85e − 1
TOU	0.0	2.37e − 3	3.33e − 2	1.36e − 1	3.18e − 1	5.32e − 1	1.51e − 1
Fromm's	0.0	1.44e − 2	2.30e − 2	7.63e − 2	2.67e − 1	5.09e − 1	1.27e − 1
QUICK	0.0	1.06e − 2	5.84e − 2	1.71e − 1	3.48e − 1	5.47e − 1	1.72e − 1
LSR(0)	0.0	1.41e − 2	1.79e − 2	8.00e − 2	2.85e − 1	5.42e − 1	1.34e − 1
LSR(−1)	0.0	6.38e − 2	1.68e − 1	1.55e − 1	1.89e − 1	5.16e − 1	1.67e − 1

case with increased $2\Delta x/\lambda$. As expected, both cases exhibit clear dependence of the discrete phase speed with signal wavelength with the discrete phase speed tending to the continuous value for long wavelengths.

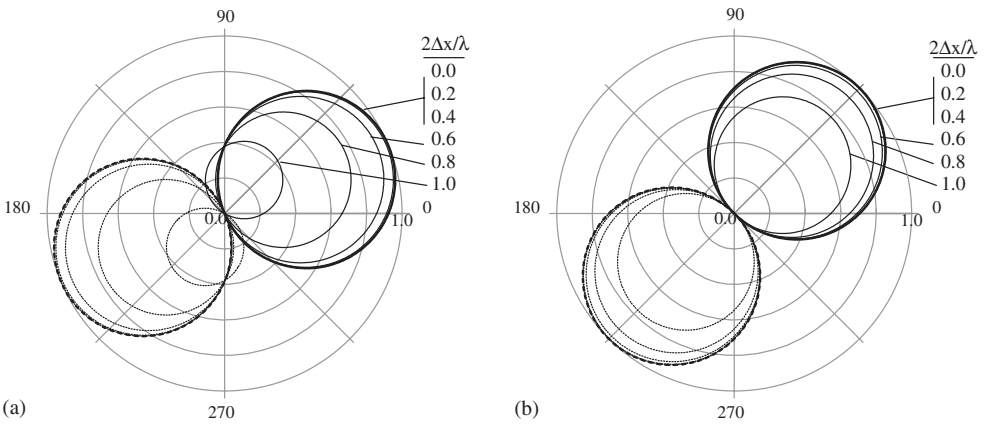

Figure 16. Non-dimensional phase speed ($\tilde{c}/\|\mathbf{u}\|$) for the consistent mass finite element method (FEM-$\mathbf{M}_c$) as a function of ϑ (azimuthal) for wave vector angles of (a) $\theta = \pi/8$ and (b) $\theta = \pi/4$ for an aspect ratio of $\gamma = 1$. Negative and positive phase speed values are shown as solid and dashed-lines respectively while the superposed bold lines show the analytic solution ($c/\|\mathbf{u}\|$).

3.2. Discrete diffusivity

This section begins with a presentation of the analytic expressions for the dimensionless discrete diffusivity for all the semi-discretizations considered. A summary of the discrete diffusivity results in terms of polar plots and the anisotropy and error metrics follows.

Discrete diffusivity formulae. Some, but not all, of the two-dimensional formulae for discrete diffusivity can be written in the same form as for phase error, Equation (7), if we replace $F_{\tilde{c}}^{1D}$ with the one-dimensional formula for dimensionless discrete diffusivity, $F_{\tilde{\alpha}}^{1D}$, given in Table VI of Part I. The result is

$$\frac{\tilde{\alpha}}{\alpha} = \cos^2\theta F_{\tilde{\alpha}}^{1D}(k\Delta x\cos\theta) + \sin^2\theta F_{\tilde{\alpha}}^{1D}(\gamma k\Delta x\sin\theta) \tag{22}$$

The methods which have this form include all of the FDMs (CD, FOU, SOU, TOU, QUICK, and Fromm) and the LSR schemes, because they all share the same 5-point CD diffusion stencil and mass matrix. Although they do not share similar operators, FEM and CVFEM can also be written in the form of Equation (22).

From Part I, the one-dimensional discrete diffusivity for FEM or CVFEM may be written in terms of φ as

$$F_{\tilde{\alpha}}^{1D} = \frac{2(1-\cos\varphi)}{\varphi^2}\,\frac{1}{\mathscr{M}(\varphi)}$$

Substitution into Equation (22) yields the two-dimensional formula for FEM/CVFEM,

$$\frac{\tilde{\alpha}}{\alpha} = \cos^2\theta\,\frac{2(1-\cos(k\Delta x\cos\theta))}{(k\Delta x\cos\theta)^2}\,\frac{1}{\mathscr{M}(\theta_x)} + \sin^2\theta\,\frac{2(1-\cos(\gamma k\Delta x\sin\theta))}{(\gamma k\Delta x\sin\theta)^2}\,\frac{1}{\mathscr{M}(\theta_y)} \tag{23}$$

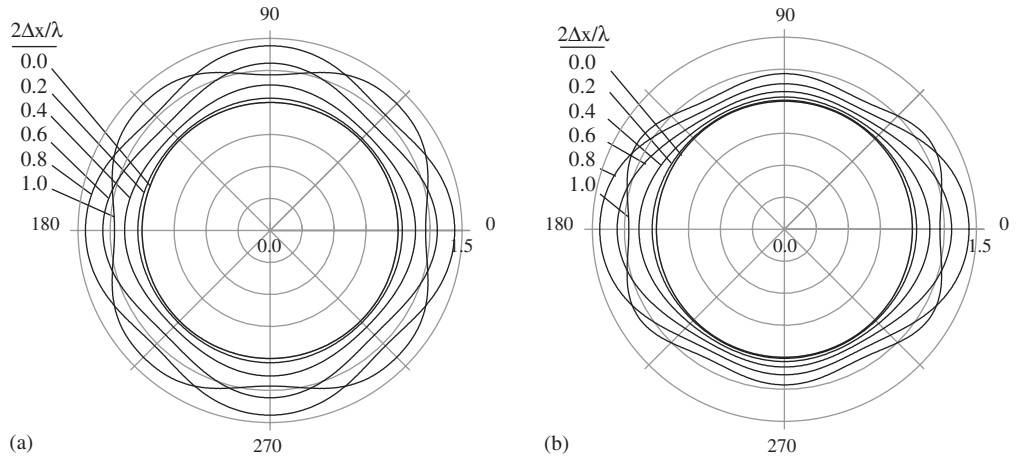

Figure 17. Non-dimensional discrete diffusivity for the consistent mass Galerkin finite element method with (a) $\gamma = 1$ and (b) $\gamma = \frac{1}{2}$.

Notice that the discrete diffusivities represented by Equation (22) degenerate to the one-dimensional form when the wave is propagating in a direction normal to the grid diagonals, i.e. when $\theta = \theta^* = \arctan(1/\gamma)$. In this case Equation (22) becomes the one-dimensional version of discrete diffusivity,

$$\frac{\tilde{\alpha}}{\alpha} = F_{\tilde{\alpha}}^{1D}(k\Delta x \cos\theta^*) \tag{24}$$

on an effective mesh spacing of $k\Delta x \cos\theta^*$, the spacing between grid diagonals.

The two-dimensional discrete diffusivity for SUPG and SUCV is

$$\frac{\tilde{\alpha}}{\alpha} = \frac{[\cos^2\theta\mathscr{F}(\theta_x)/\theta_x^2 + \sin^2\theta\mathscr{F}(\theta_y)/\theta_y^2]}{[1+\beta^2(\theta_x+\theta_y)^2(\cos^2\theta\mathscr{G}(\theta_x) + \sin^2\theta\mathscr{G}(\theta_y))^2]} \tag{25}$$

in terms of the functions defined in Equation (19).

Discrete diffusivity results. The discrete diffusivity results for our two-dimensional semi-discretizations are presented in Figures 17–24. Figures (a) and (b) present $\tilde{\alpha}/\alpha$ for grid aspect ratios of $\gamma = 1$ and $\frac{1}{2}$, respectively. Dimensionless discrete diffusivity curves are plotted for $2\Delta x/\lambda = 0$, 0.2, 0.4, 0.6, 0.8 and 1.0. In the ideal case, the discrete diffusivity would exactly replicate the continuous diffusivity for the entire discrete spectrum from the limit $2\Delta x/\lambda \to 0$ to the grid Nyquist limit. Hence, in the ideal case, the discrete diffusivity curves would be circular, each giving $\tilde{\alpha}/\alpha = 1$. However, all of the methods considered here are either over- or under-diffusive, the magnitude of the error in diffusivity being dependent on wavelength, grid aspect ratio and propagation direction.

Several points regarding the semi-discretizations are noted before beginning the discussion of results. First, results for the lumped mass variants of FEM and CVFEM are not included here because their results are significantly degraded relative to their consistent mass counterparts. Second, as the finite difference semi-discretizations use second-order centred approximations for the diffusion operator in conjunction with a lumped mass matrix, they

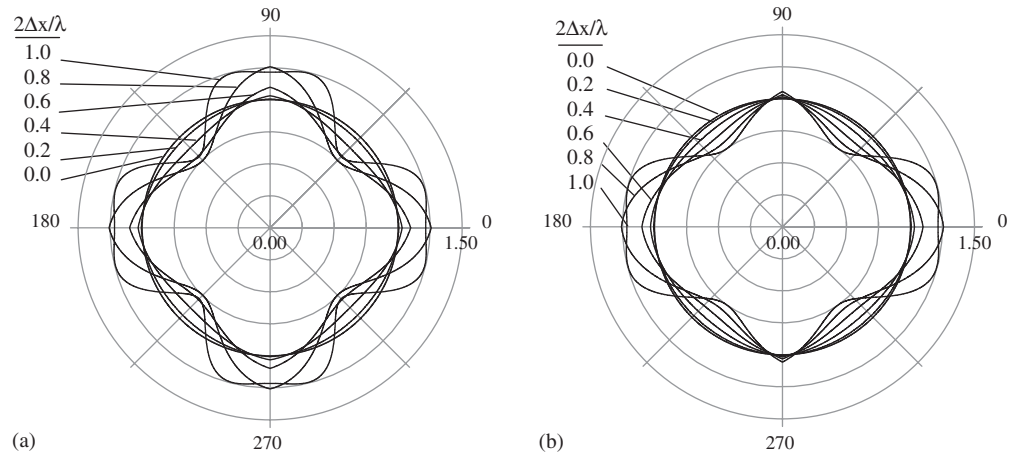

Figure 18. Non-dimensional discrete diffusivity ($\tilde{\alpha}/\alpha$; radial) as a function of θ (azimuthal) for consistent mass matrix finite element method SUPG with β_{opt} with (a) $\gamma = 1$ and (b) $\gamma = \frac{1}{2}$.

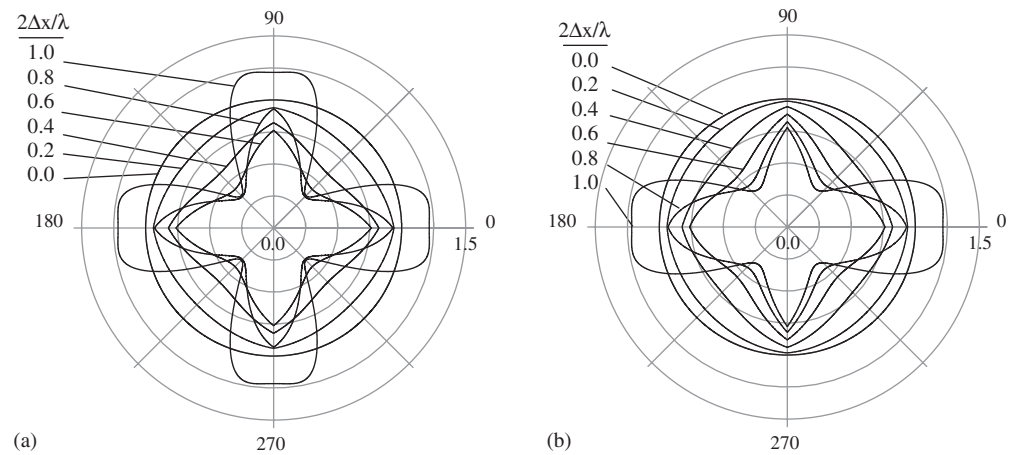

Figure 19. Non-dimensional discrete diffusivity ($\tilde{\alpha}/\alpha$; radial) as a function of θ (azimuthal) for consistent mass matrix finite element method SUPG with $\beta = \frac{1}{2}$ with (a) $\gamma = 1$ and (b) $\gamma = \frac{1}{2}$.

yield identical discrete diffusivities (the exception being CD-$\mathbf{M}_c$ where the 'consistent' mass matrix is used). For this reason, discrete diffusivity results for the lumped mass finite difference schemes considered here are identical and presented as one result labeled FDM.

Several characteristics are evident from the series of figures presented here. First, the figures clearly indicate anisotropic discrete diffusivities for all schemes considered. As with the two-dimensional phase speed results, the $\gamma = 1$ cases all show quarter-symmetry while the $\gamma = \frac{1}{2}$ discretizations show half-symmetry. The figures also suggest that the anisotropy generally increases with increasing $2\Delta x/\lambda$. This observation is demonstrated quantitatively in

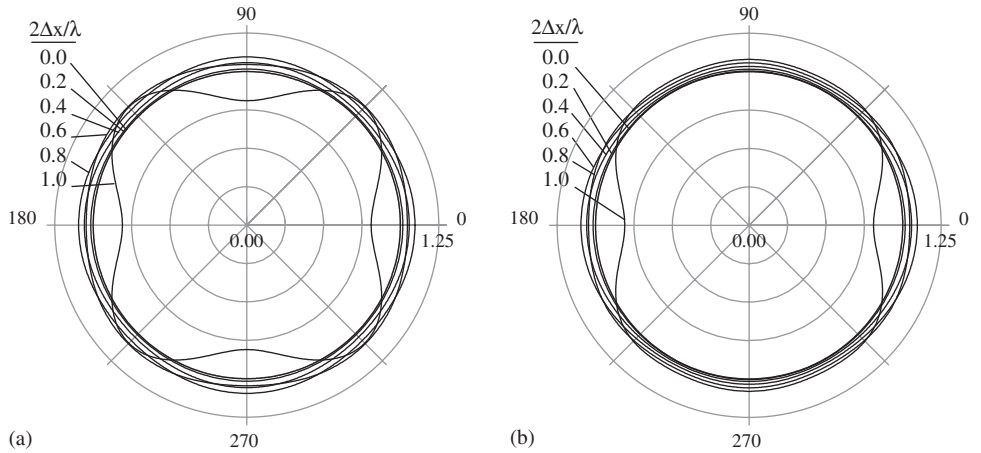

Figure 20. Non-dimensional discrete diffusivity for the consistent mass control volume finite element method with (a) $\gamma = 1$ and (b) $\gamma = \frac{1}{2}$.

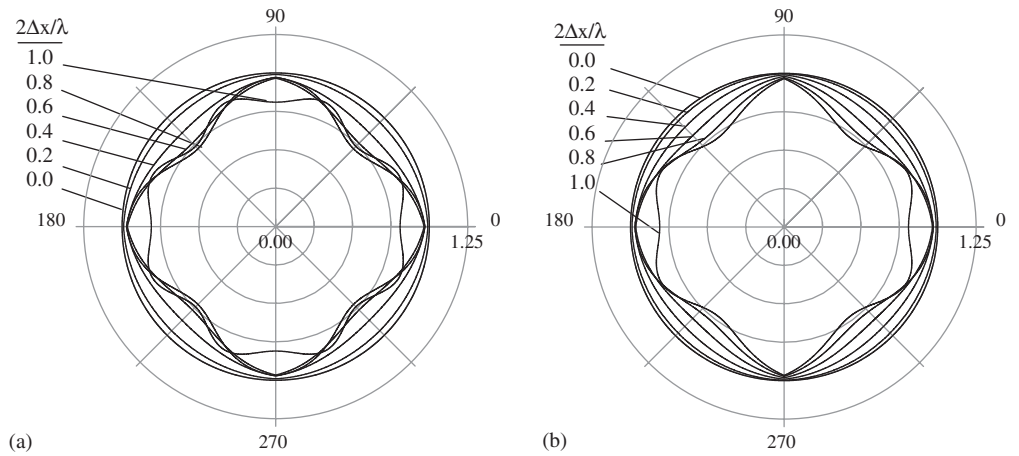

Figure 21. Non-dimensional discrete diffusivity ($\tilde{\alpha}/\alpha$; radial) as a function of θ (azimuthal) for consistent mass matrix control volume finite element method SUCV with β_{opt} with (a) $\gamma = 1$ and (b) $\gamma = \frac{1}{2}$.

Tables V and VI where the coefficient of variation of the discrete diffusivity, $\varsigma_{\tilde{\alpha}}$, and its mean, $\overline{\varsigma_{\tilde{\alpha}}}$, are presented. The tables show that $\varsigma_{\tilde{\alpha}}$ generally grows with increasing dimensionless wave number. In terms of the $\overline{\varsigma_{\tilde{\alpha}}}$ metric, and relative to the grid aspect ratio, $\gamma = \frac{1}{2}$ minimizes θ-dependence for all but the FEM-$\mathbf{M}_c$ and SUCV $\beta = \frac{1}{2}$ semi-discretizations. Finally, it is evident from a method-to-method comparison of $\overline{\varsigma_{\tilde{\alpha}}}$ that FEM-$\mathbf{M}_c$ and CVFEM-$\mathbf{M}_c$ minimize anisotropic behaviour regardless of grid aspect ratio. Note that the SUCV and SUPG schemes can achieve equal or better anisotropy performance relative to FEM and CVFEM given the proper choice of β though a poor choice yields the overall worst anisotropy. It is also

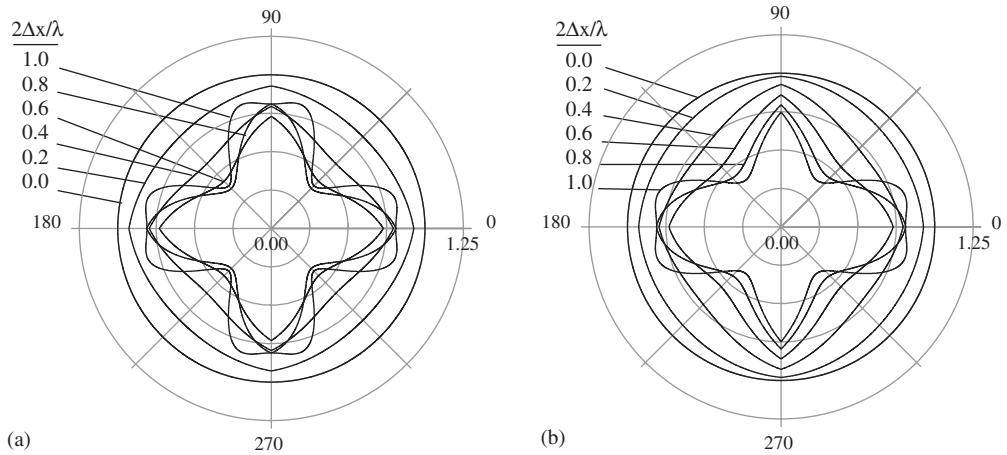

Figure 22. Non-dimensional discrete diffusivity ($\tilde{\alpha}/\alpha$; radial) as a function of θ (azimuthal) for consistent mass matrix control volume finite element method SUCV with $\beta = \frac{1}{2}$ with (a) $\gamma = 1$ and (b) $\gamma = \frac{1}{2}$.

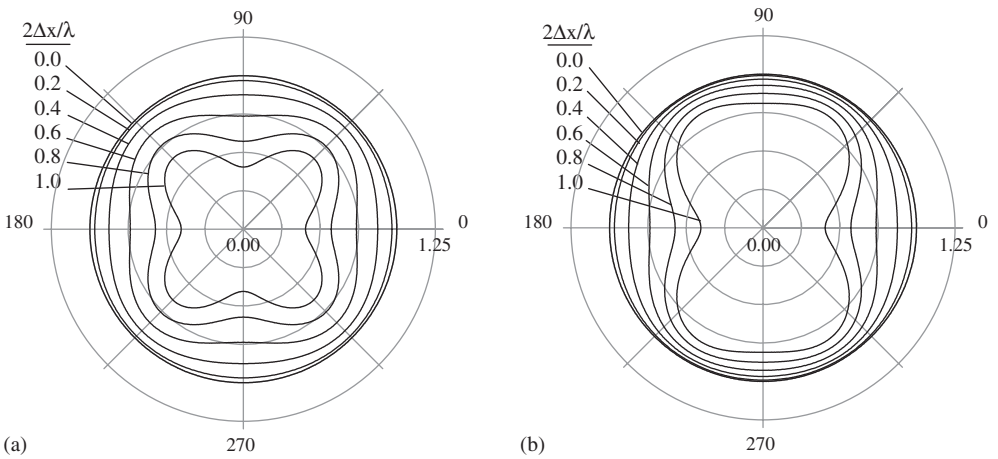

Figure 23. Non-dimensional discrete diffusivity for the finite difference method (FDM, 5-point stencil) with aspect ratios of (a) $\gamma = 1$ and (b) $\gamma = \frac{1}{2}$.

interesting to note that the best choice of stabilization parameter for SUCV ($\beta = \frac{1}{2}$) in terms of phase speed anisotropy (cf. Tables VII and VIII) is the worst choice for discrete diffusivity for that method. A similar property holds for SUPG with $\beta = \beta_{\text{opt}}$.

The series of figures in this section also provides information concerning the error in the discrete diffusivity relative to its continuum counterpart for each method. As suggested by the anisotropy discussion above, this error is dependent on wave number as well as propagation angle. A quantitative measure of the discrete diffusivity errors is presented in Tables VII and VIII. As with $\varsigma_{\tilde{\alpha}}$, the discrete diffusivity errors, $\varepsilon_{\tilde{\alpha}}$, generally increase with increasing $2\Delta x/\lambda$,

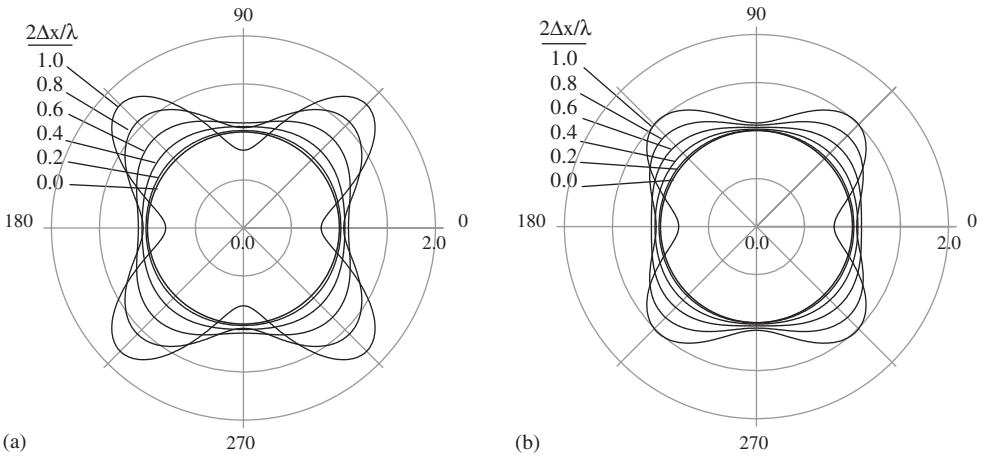

Figure 24. Non-dimensional discrete diffusivity ($\tilde{\alpha}/\alpha$; radial) as a function of θ (azimuthal) for the node-centred finite volume method with second order gradient approximation and consistent mass matrix (CD-$\mathbf{M}_c$) with (a) $\gamma = 1$ and (b) $\gamma = \frac{1}{2}$.

peaking at the Nyquist limit. In terms of the $\overline{\varepsilon_{\tilde{\alpha}}}$ metric, the $\gamma = \frac{1}{2}$ results minimize diffusivity errors relative to the unit aspect ratio cases for all the methods. Finally, it is evident from a method-to-method comparison of $\overline{\varepsilon_{\tilde{\alpha}}}$ that CVFEM-$\mathbf{M}_c$ minimizes errors, irrespective of γ. Note that the SUPG and SUCV semi-discretizations yield by far the worst discrete diffusivity error (in terms of $\overline{\varepsilon_{\tilde{\alpha}}}$) relative to the other semi-discretizations, irrespective of aspect ratio.

3.3. *Artificial diffusivity*

This section examines artificial diffusivity associated with our two-dimensional semi-discretizations. As noted in Part I, artificial diffusion may be added deliberately (e.g. SUPG/SUCV) or be a by-product of the discretization (e.g. first-order upwind). While in general not a desirable feature of a method, artificial diffusivity can be used to stabilize a discretization scheme. In terms of artificial diffusivity, stabilization is achieved through the annihilation (damping) of numerical artifacts such as short wavelength dispersion errors in under-resolved convection-dominated problems. In this light, an ideal artificial diffusivity function for either one- or two-dimensional discretizations would only be active in the large wave number part of the discrete spectrum, near the Nyquist limit for example, and be negligible otherwise, going to zero at the long wavelength limit. For two-dimensional discretizations, it is also desirable that the artificial diffusivity have an angular variation similar to the angular variation observed in the phase error so that short wavelength dispersion errors are damped at the same rate, regardless of propagation direction.

This section begins with a presentation of the analytic expressions for the non-dimensional artificial diffusivity, presented in terms of $1/\mathbf{P}_e^{\text{art}}$ ($= 2\alpha_{\text{art}}/c\Delta x$), for all the semi-discrete methods considered. A summary of the artificial diffusivity results in terms of polar plots and error metrics follows.

Artificial diffusivity formulae. As was the case for several of the previously discussed two-dimensional discrete phase speed and diffusivity formulae, the two-dimensional formulae for

Table V. Coefficient of variation of discrete diffusivity, $\varsigma_{\tilde{\alpha}}$, as a function of $2\Delta x/\lambda$, and its average, $\overline{\varsigma_{\tilde{\alpha}}}$, for the two-dimensional, $\gamma = 1$, semi-discretization considered here.

	$\varsigma_{\tilde{\alpha}}$ as a function of $2\Delta x/\lambda$						
Method	0.0	0.2	0.4	0.6	0.8	1.0	$\overline{\varsigma_{\tilde{\alpha}}}$
FEM-$\mathbf{M}_c$	0.0	5.78e − 3	2.24e − 2	4.38e − 2	4.35e − 2	5.07e − 2	2.82e − 2
SUPG β_{opt}	0.0	1.35e − 2	5.09e − 2	1.07e − 1	1.79e − 1	1.56e − 1	8.57e − 2
SUPG $\beta = \frac{1}{2}$	0.0	3.22e − 2	1.02e − 1	1.89e − 1	3.32e − 1	4.07e − 1	1.72e − 1
CVFEM-$\mathbf{M}_c$	0.0	5.85e − 3	2.37e − 2	5.47e − 2	1.01e − 1	1.64e − 1	5.34e − 2
SUCV β_{opt}	0.0	1.06e − 2	3.85e − 2	7.58e − 2	1.04e − 1	5.08e − 2	5.08e − 2
SUCV $\beta = \frac{1}{2}$	0.0	2.17e − 3	4.37e − 3	1.77e − 2	4.92e − 2	5.81e − 1	7.28e − 2
FDM	0.0	1.19e − 2	5.06e − 2	1.29e − 1	2.85e − 1	7.00e − 1	1.65e − 1
CD-$\mathbf{M}_c$	0.0	1.19e − 2	5.21e − 2	1.38e − 1	3.22e − 1	7.60e − 1	1.81e − 1

Table VI. Coefficient of variation of discrete diffusivity, $\varsigma_{\tilde{\alpha}}$, as a function of $2\Delta x/\lambda$, and its average, $\overline{\varsigma_{\tilde{\alpha}}}$, for the two-dimensional, $\gamma = \frac{1}{2}$ semi-discretizations considered here.

	$\varsigma_{\tilde{\alpha}}$ as a function of $2\Delta x/\lambda$						
Method	0.0	0.2	0.4	0.6	0.8	1.0	$\overline{\varsigma_{\tilde{\alpha}}}$
FEM-$\mathbf{M}_c$	0.0	9.45e − 3	3.73e − 2	7.78e − 2	1.01e − 1	4.29e − 2	4.94e − 2
SUPG β_{opt}	0.0	7.78e − 3	3.10e − 2	7.29e − 2	1.48e − 1	1.84e − 1	7.03e − 2
SUPG $\beta = \frac{1}{2}$	0.0	2.37e − 2	7.73e − 2	1.34e − 1	2.43e − 1	4.48e − 1	1.40e − 1
CVFEM-$\mathbf{M}_c$	0.0	4.56e − 3	1.58e − 2	2.34e − 2	7.75e − 3	9.27e − 2	1.96e − 2
SUCV β_{opt}	0.0	6.21e − 3	2.30e − 2	4.78e − 2	7.76e − 2	7.71e − 2	3.86e − 2
SUCV $\beta = \frac{1}{2}$	0.0	2.51e − 2	7.76e − 2	1.26e − 1	2.01e − 1	2.80e − 1	1.14e − 1
FDM	0.0	9.46e − 3	3.78e − 2	8.47e − 2	1.49e − 1	2.30e − 1	7.92e − 2
CD-$\mathbf{M}_c$	0.0	5.58e − 3	2.12e − 2	4.48e − 2	8.54e − 2	1.79e − 1	4.94e − 2

Table VII. RMS discrete diffusivity error, $\varepsilon_{\tilde{\alpha}}$, as a function of $2\Delta x/\lambda$, and its average, $\overline{\varepsilon_{\tilde{\alpha}}}$, for the two-dimensional, $\gamma = 1$ semi-discretizations considered here.

	$\varepsilon_{\tilde{\alpha}}$ as a function of $2\Delta x/\lambda$						
Method	0.0	0.2	0.4	0.6	0.8	1.0	$\overline{\varepsilon_{\tilde{\alpha}}}$
FEM-$\mathbf{M}_c$	0.0	2.56e − 2	1.05e − 1	2.38e − 1	3.70e − 1	3.26e − 1	1.80e − 1
SUPG β_{opt}	0.0	2.18e − 2	7.37e − 2	1.26e − 1	1.76e − 1	1.88e − 1	9.84e − 2
SUPG $\beta = \frac{1}{2}$	0.0	1.20e − 1	3.28e − 1	4.61e − 1	4.63e − 1	3.78e − 1	3.12e − 1
CVFEM-$\mathbf{M}_c$	0.0	1.24e − 2	4.56e − 2	8.06e − 2	7.19e − 2	1.12e − 1	5.33e − 2
SUCV β_{opt}	0.0	3.04e − 2	9.92e − 2	1.60e − 1	1.79e − 1	1.84e − 1	1.12e − 1
SUCV $\beta = \frac{1}{2}$	0.0	1.28e − 1	3.37e − 1	4.60e − 1	4.65e − 1	3.81e − 1	3.16e − 1
FDM	0.0	2.51e − 2	9.69e − 2	2.06e − 1	3.39e − 1	4.79e − 1	1.81e − 1
CD-$\mathbf{M}_c$	0.0	2.54e − 2	1.01e − 1	2.19e − 1	3.49e − 1	4.51e − 1	1.84e − 1

Table VIII. RMS discrete diffusivity error, $\varepsilon_{\tilde{\alpha}}$, as a function of $2\Delta x/\lambda$, and its average, $\overline{\varepsilon_{\tilde{\alpha}}}$, for the two-dimensional, $\gamma = \frac{1}{2}$ semi-discretizations considered here.

	$\varepsilon_{\tilde{\alpha}}$ as a function of $2\Delta x/\lambda$						
Method	0.0	0.2	0.4	0.6	0.8	1.0	$\overline{\varepsilon_{\tilde{\alpha}}}$
FEM-$\mathbf{M}_c$	0.0	1.83e − 2	7.50e − 2	1.70e − 1	2.65e − 1	2.46e − 1	1.30e − 1
SUPG β_{opt}	0.0	1.19e − 2	4.32e − 2	8.57e − 2	1.47e − 1	1.82e − 1	7.57e − 2
SUPG $\beta = \frac{1}{2}$	0.0	7.37e − 2	2.26e − 1	3.56e − 1	4.15e − 1	4.38e − 1	2.58e − 1
CVFEM-$\mathbf{M}_c$	0.0	8.86e − 3	3.27e − 2	5.86e − 2	5.79e − 2	9.32e − 2	4.09e − 2
SUCV β_{opt}	0.0	1.75e − 2	6.11e − 2	1.11e − 1	1.50e − 1	1.91e − 1	8.70e − 2
SUCV $\beta = \frac{1}{2}$	0.0	7.96e − 2	2.37e − 1	3.64e − 1	4.25e − 1	4.43e − 1	2.65e − 1
FDM	0.0	1.79e − 2	6.92e − 2	1.48e − 1	2.43e − 1	3.46e − 1	1.30e − 1
CD-$\mathbf{M}_c$	0.0	1.64e − 2	6.44e − 2	1.38e − 1	2.19e − 1	3.05e − 1	1.18e − 1

artificial diffusivity for SOU, TOU, Fromm, and QUICK can be written in the form

$$\frac{2\alpha_{\text{art}}}{c} = (\Delta x \cos\theta)\cos^2\theta F^{1D}_{\alpha_{\text{art}}}(k\Delta x\cos\theta) + (\Delta y \sin\theta)\sin^2\theta F^{1D}_{\alpha_{\text{art}}}(k\Delta y\sin\theta) \tag{26}$$

where $F^{1D}_{\alpha_{\text{art}}}(\varphi)$ denotes the dimensionless one-dimensional formula for artificial diffusivity as given in Table VIII of Part I. In terms of the $\mathbf{P}^{\text{art}}_e$ defined previously, the formula becomes

$$\frac{1}{\mathbf{P}^{\text{art}}_e} = \cos^3\theta F^{1D}_{\alpha_{\text{art}}}(k\Delta x\cos\theta) + \gamma\sin^3\theta F^{1D}_{\alpha_{\text{art}}}(\gamma k\Delta x\sin\theta) \tag{27}$$

When $\theta = \theta^* = \arctan(1/\gamma)$ (i.e. waves are propagating perpendicular to mesh diagonals) Equation (27) reverts to the one-dimensional version with an effective mesh spacing $(\Delta x\cos\theta^*)$

$$\frac{1}{\mathbf{P}^{\text{art}}_e\cos\theta^*} = \frac{2\alpha_{\text{art}}}{c\Delta x\cos\theta^*} = F^{1D}_{\alpha_{\text{art}}}(k\Delta x\cos\theta^*) \tag{28}$$

Note that Equation (28) also includes the effective grid spacing in the definition of an effective Peclet number, $\mathbf{P}^{\text{art}}_e\cos\theta^*$.

The remaining schemes do not have as simple a form as Equation (27); these include the LSR schemes, SUPG and SUCV. Dimensionless artificial diffusivity for the LSR(−1) scheme is

$$\frac{1}{\mathbf{P}^{\text{art}}_e} = \frac{\cos^2\theta}{3\theta_x^2}[11 + (1 + 2\cos\theta_y)\cos 2\theta_x - 12\cos\theta_x - 2\cos\theta_y] + \frac{\sin^2\theta}{3\theta_y^2}[11 + (1 + 2\cos\theta_x)\cos 2\theta_y - 12\cos\theta_y - 2\cos\theta_x] \tag{29}$$

Along the co-ordinate directions this reduces to the artificial diffusion formula for SOU. The two-dimensional artificial diffusion formula for LSR(0) is $\frac{1}{2}$ times the formula for LSR(−1).

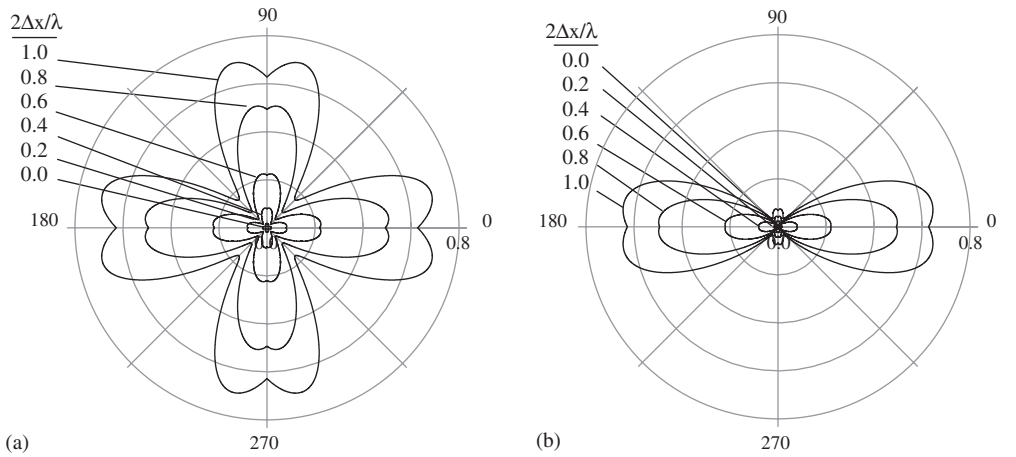

Figure 25. Non-dimensional artificial diffusivity ($1/\mathbf{P}_e^{\text{art}}$; radial) as a function of θ (azimuthal) for consistent mass matrix finite element method SUPG with β_{opt} for (a) $\gamma = 1$ and (b) $\gamma = \frac{1}{2}$.

Along co-ordinate directions the LSR(-1) scheme reduces to the one-dimensional form which is, incidentally, also Fromm's method.

The artificial diffusivity for SUPG and SUCV is given by

$$\frac{1}{\mathbf{P}_e^{\text{art}}} = 4\beta_\theta \frac{[\cos^4\theta/\theta_x^2 \mathscr{M}(\theta_x)((1-\cos\theta_x) - \sin^2\theta/2\mathscr{M}(\theta_x)) + \sin^4\theta/\theta_y^2 \mathscr{M}(\theta_y)((1-\cos\theta_y) - \sin^2\theta/2\mathscr{M}(\theta_y))]}{[1+\beta^2(\theta_x+\theta_y)^2(\cos^2\theta\mathscr{G}(\theta_x) + \sin^2\theta\mathscr{G}(\theta_y))^2]} \tag{30}$$

in terms of the definitions in Equation (19) and the symbol for the mass matrix, $\mathscr{M}(\theta)$ given in Table I of Part I. The similarity of the various terms to the one-dimensional version is clear (see Table VIII of Part I). The formulae revert to the corresponding one-dimensional formulae along the co-ordinate directions.

Artificial diffusivity results. The artificial diffusivity results for the two-dimensional semi-discretizations are presented in Figures 25–31. Figures (a) and (b) for each method present dimensionless artificial diffusivity, $1/\mathbf{P}_e^{\text{art}}$, for grid aspect ratios of $\gamma = 1$ and $\frac{1}{2}$, respectively. Dimensionless artificial diffusivity curves are plotted for $2\Delta x/\lambda = 0$, 0.2, 0.4, 0.6, 0.8 and 1.0.

All the methods show quarter- and half-symmetry for the $\gamma = 1$ and $\frac{1}{2}$ aspect ratio cases, respectively—consistent with the symmetry of the underlying spatial grid. Additionally, it is clear that the artificial diffusion functions in general display more anisotropy than the other dispersion and diffusion relations. This anisotropy can be understood, at least in part, by considering schemes characterized by Equation (27). Although the remaining schemes (i.e. LSR, SUPG and SUCV) incorporate cross terms (as noted in the previous discussion) their behaviour may be at least partially explained in terms of the following discussion.

With the obvious exception of FOU, the one-dimensional functions ($F^{1D}_{\alpha_{\text{art}}}$) provide significant artificial diffusion only at short wavelengths and very little at long wavelengths (see Part I). The reduced effective grid spacing ($\Delta x \cos\theta^*$) in Equation (28) accentuates this spectral character of the one-dimensional artificial diffusivity functions. The (directionally dependent) effective grid spacing skews the range of the artificial diffusivity functions toward the long

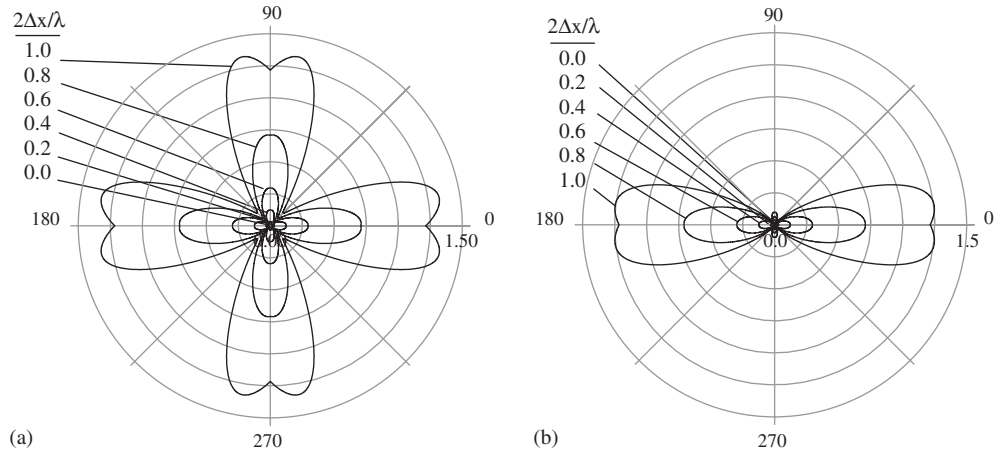

Figure 26. Non-dimensional artificial diffusivity ($1/\mathbf{P}_e^{\text{art}}$; radial) as a function of θ (azimuthal) for consistent mass matrix finite element method SUPG with $\beta = \frac{1}{2}$ for (a) $\gamma = 1$; and (b) $\gamma = \frac{1}{2}$.

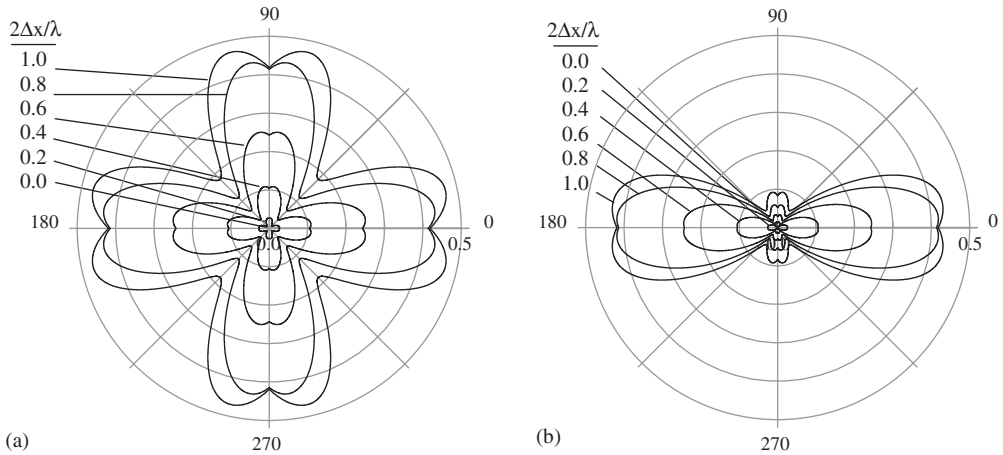

Figure 27. Non-dimensional artificial diffusivity ($1/\mathbf{P}_e^{\text{art}}$; radial) as a function of θ (azimuthal) for consistent mass matrix control volume finite element method SUCV with β_{opt} for (a) $\gamma = 1$ and (b) $\gamma = \frac{1}{2}$.

wave spectrum. For example, for $\gamma = \frac{1}{2}$ waves oriented along $\theta = \theta^* = \arctan(2)$ will experience artificial diffusivity of the form (Equation (28))

$$\frac{1}{\mathbf{P}_e^{\text{art}}} = \frac{1}{\sqrt{5}} F^{1D}_{\alpha_{\text{art}}}\left(\frac{k\Delta x}{\sqrt{5}}\right) \tag{31}$$

in which the formula is purposely scaled in terms of $\mathbf{P}_e^{\text{art}}$, as it appears in the plots. Thus, the artificial diffusivity along this direction is $1/\sqrt{5}$ of the one-dimensional function evaluated over the reduced wave number range, $0 \leqslant 2\Delta x/\lambda \leqslant 1/\sqrt{5}$; thus, artificial diffusivity is much reduced

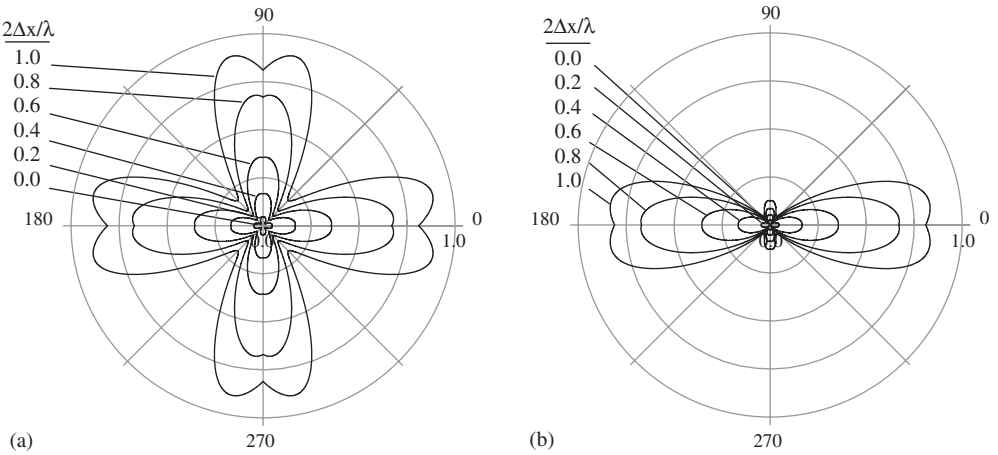

Figure 28. Non-dimensional artificial diffusivity ($1/\mathbf{P}_e^{\text{art}}$; radial) as a function of θ (azimuthal) for consistent mass matrix control volume finite elementmethod SUCV with $\beta = \frac{1}{2}$ for (a) $\gamma = 1$ and (b) $\gamma = \frac{1}{2}$ (right).

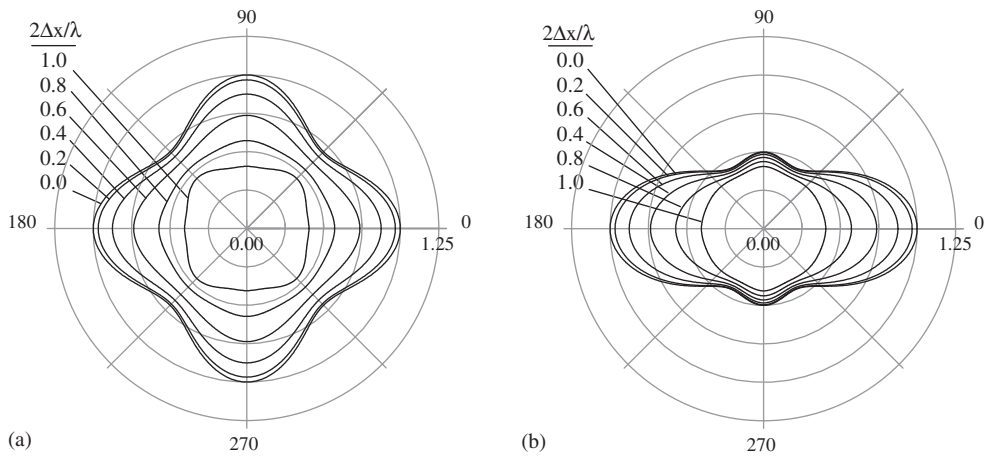

Figure 29. Non-dimensional artificial diffusivity ($1/\mathbf{P}_e^{\text{art}}$; radial) as a function of θ (azimuthal) for the first-order upwind (FOU) semi-discretization. Results for aspect ratios of (a) $\gamma = 1$ and (b) $\gamma = \frac{1}{2}$ are shown.

in this direction as compared to the horizontal direction. However, the phase error in this direction will also be less relative to the horizontal direction (see Equation (7)), therefore much less artificial diffusivity is needed in this direction. Indeed, the figures demonstrate that artificial diffusivity is generally maximized along the x- and y-coordinate directions when $\gamma = 1$, and along the x-coordinate direction for $\gamma = \frac{1}{2}$. Recall that these directions correspond to the worst phase speed accuracy for each of these aspect ratios. For methods characterized by Equation

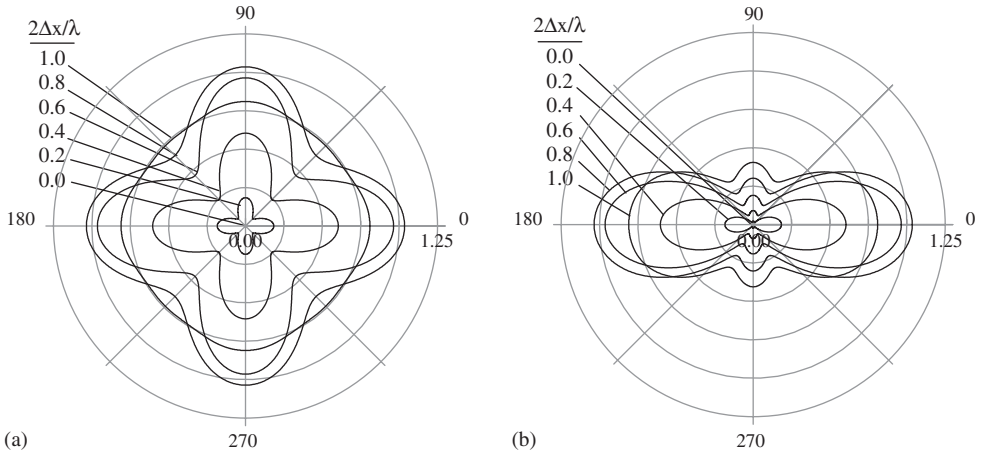

Figure 30. Non-dimensional artificial diffusivity ($1/\mathbf{P}_e^{\text{art}}$; radial) as a function of θ (azimuthal) for the second-order upwind (SOU) semi-discretization. Results are shown for (a) $\gamma = 1$ and (b) $\gamma = \frac{1}{2}$. The figure also depicts artificial diffusivity for TOU, QUICK, and Fromm's method, with a scaled radial coordinate, see Equation (27) and Table VIII of Part I. The plots show $3/\mathbf{P}_e^{\text{art}}$ for TOU, $4/\mathbf{P}_e^{\text{art}}$ for QUICK, and $2/\mathbf{P}_e^{\text{art}}$ for Fromm's method.

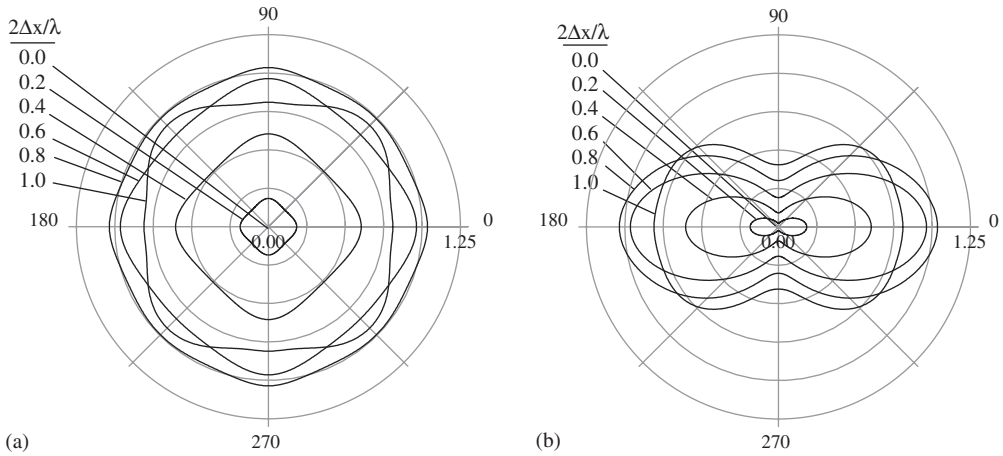

Figure 31. Non-dimensional artificial diffusivity ($1/\mathbf{P}_e^{\text{art}}$; radial) as a function of θ (azimuthal) for the least squares reconstruction method, LSR(-1). Results for (a) $\gamma = 1$ and (b) $\gamma = \frac{1}{2}$ are shown. The figure also shows $2/\mathbf{P}_e^{\text{art}}$ for the LSR(0) least squares reconstruction method, i.e. the artificial diffusion for LSR(0) is one-half that of LSR(-1), see Equation (27) and Table VIII of Part I.

(27), artificial diffusivity is generally minimized along the $\theta = \theta^*$ direction, corresponding to the best dispersion accuracy for those same methods. Clearly, the anisotropy of the artificial diffusivity is consistent with the anisotropy of the concomitant dispersive behaviour. Hence, coefficient of variation is not an appropriate metric for comparing methods and is not shown.

Table IX. RMS value of the dimensionless artificial diffusivity, ε_{art}, as a function of $2\Delta x/\lambda$, and its average, $\overline{\varepsilon_{art}}$, for the two-dimensional $\gamma = 1$ semi-discretizations considered here.

	ε_{art} as a function of $2\Delta x/\lambda$						
Method	0.0	0.2	0.4	0.6	0.8	1.0	$\overline{\varepsilon_{art}}$
SUPG β_{opt}	0.0	1.40e − 2	6.03e − 2	1.57e − 1	3.48e − 1	5.29e − 1	1.69e − 1
SUPG $\beta = \frac{1}{2}$	0.0	2.47e − 2	8.66e − 2	1.92e − 1	4.36e − 1	9.13e − 1	2.39e − 1
SUCV β_{opt}	0.0	2.04e − 2	8.06e − 2	1.81e − 1	3.14e − 1	3.75e − 1	1.57e − 1
SUCV $\beta = \frac{1}{2}$	0.0	3.60e − 2	1.19e − 1	2.39e − 1	4.45e − 1	6.50e − 1	2.33e − 1
FOU	8.55e − 1	8.32e − 1	7.67e − 1	6.69e − 1	5.50e − 1	4.26e − 1	6.92e − 1
SOU	0.0	1.33e − 1	4.46e − 1	7.42e − 1	8.58e − 1	7.68e − 1	5.13e − 1
TOU	0.0	4.44e − 2	1.49e − 1	2.47e − 1	2.86e − 1	2.56e − 1	1.71e − 1
Fromm's	0.0	6.67e − 2	2.23e − 1	3.71e − 1	4.29e − 1	3.84e − 1	2.56e − 1
QUICK	0.0	3.34e − 2	1.12e − 1	1.86e − 1	2.15e − 1	1.92e − 1	1.28e − 1
LSR(0)	0.0	8.39e − 2	2.76e − 1	4.47e − 1	5.00e − 1	4.31e − 1	3.05e − 1
LSR(−1)	0.0	1.68e − 1	5.52e − 1	8.95e − 1	1.00	8.63e − 1	6.09e − 1

Table X. RMS value of the dimensionless artificial diffusivity, ε_{art}, as a function of $2\Delta x/\lambda$, and its average, $\overline{\varepsilon_{art}}$, for the two-dimensional $\gamma = 1$ semi-discretizations considered here.

	ε_{art} as a function of $2\Delta x/\lambda$						
Method	0.0	0.2	0.4	0.6	0.8	1.0	$\overline{\varepsilon_{art}}$
SUPG β_{opt}	0.0	9.07e − 3	3.98e − 2	1.06e − 1	2.34e − 1	3.44e − 1	1.12e − 1
SUPG $\beta = \frac{1}{2}$	0.0	1.63e − 2	6.00e − 2	1.36e − 1	3.09e − 1	6.08e − 1	1.65e − 1
SUCV β_{opt}	0.0	1.32e − 2	5.31e − 2	1.21e − 1	2.09e − 1	2.42e − 1	1.03e − 1
SUCV $\beta = \frac{1}{2}$	0.0	2.38e − 2	8.19e − 2	1.68e − 1	3.09e − 1	4.28e − 1	1.59e − 1
FOU	6.66e − 1	6.51e − 1	6.09e − 1	5.45e − 1	4.70e − 1	3.92e − 1	5.61e − 1
SOU	0.0	9.36e − 2	3.13e − 1	5.21e − 1	6.08e − 1	5.62e − 1	3.63e − 1
TOU	0.0	3.12e − 2	1.04e − 1	1.74e − 1	2.03e − 1	1.87e − 1	1.21e − 1
Fromm's	0.0	4.68e − 2	1.57e − 1	2.61e − 1	3.04e − 1	2.81e − 1	1.82e − 1
QUICK	0.0	2.34e − 2	7.83e − 2	1.30e − 1	1.52e − 1	1.40e − 1	9.09e − 2
LSR(0)	0.0	5.18e − 2	1.74e − 1	2.95e − 1	3.53e − 1	3.41e − 1	2.09e − 1
LSR(−1)	0.0	1.04e − 1	3.49e − 1	5.89e − 1	7.05e − 1	6.82e − 1	4.18e − 1

The series of figures in this section provides information concerning the magnitude of the artificial diffusivity of each method. A quantitative measure of the dimensionless integrated (over orientation and wave number) artificial diffusivity is presented in Tables IX and X for the $\gamma = 1$ and $\frac{1}{2}$ aspect ratio cases, respectively. All but the FOU semi-discretizations demonstrate generally increasing artificial diffusivity, in terms of the ε_{art} metric, with increasing wave number. As with the one-dimensional results, FOU exhibits dimensionless artificial diffusivity which *decreases* with the wave number. In terms of the $\overline{\varepsilon_{art}}$ metric, the FOU and LSR(−1) methods show the greatest amount of damping while the QUICK scheme produces the least artificial diffusivity as measured in this metric.

4. SUMMARY AND CONCLUSIONS

4.1. Summary

In this two-part paper, we have presented a multi-methods comparison of a variety of popular discretization schemes in the context of linear advection–diffusion. As the starting point for this multi-methods analysis and comparison, we chose to apply Fourier analysis because it provides a general methodology that is capable of analysing multiple methods in a single mathematical framework while providing a great deal of information and insight into each method. In this work, Fourier analysis has been used to investigate the following aspects of each numerical method: (a) numerical dispersion, i.e. phase and group velocity errors, (b) the spectral behaviour of the discrete diffusivity, (c) the limiting behaviour of short wavelength information for both wave propagation and diffusion, (d) the identification and characterization of artificial diffusivity introduced via upwinding, (e) grid bias errors in phase, discrete diffusivity and artificial diffusivity, and (f) asymptotic convergence properties and resolution requirements.

The results of this analysis show that there are a number of competing methods that are all of second-order accuracy or better and that should perform adequately in the hands of an experienced analyst. While there is no *single* best method identified, there are at least two methods that are clearly the worst. The first-order upwind method is excessively diffusive, and the second-order upwind method is extremely dispersive—as are the FEM-SUPG and CVFEM-SUCV methods at low Peclet number.

The Galerkin finite element method and its streamline-upwind derivatives exhibit super-convergent behaviour in terms of dispersive behaviour, i.e. phase and group accuracy. The only other method considered that exhibited this behaviour is the third-order upwind scheme. Analysis of several CVFEM methods and their streamline-upwind derivatives revealed that their behaviour is strictly second-order in all of our metrics. While it appears that these methods yield good phase and group accuracy when the accuracy requirements are relaxed, the resolution requirements for an acceptable 1% error in phase and group is more than twice that of the finite element method in a one-dimensional sense (greater than a factor of eight in three dimensions).

The deleterious effects of *ad hoc* mass-lumping was demonstrated (again) for the FEM and CVFEM formulations. In comparison, the FDM and FVM formulations, by default, incorporate a diagonal mass matrix, i.e. they come equipped with a built-in lumped mass approximation in which the nodal time derivatives are decoupled. In terms of advection-diffusion, the FDM and FVM schemes represent the time-dependent terms by an equivalent lumped-capacitance. In contrast, the consistent mass matrix inherent in the FEM/CVFEM formulations represent these time-dependent terms by a distributed capacitance that more accurately reflects the physical situation in the continuum. As a consequence, the lumped-capacitance representation inherent in the FDM and FVM schemes yield schemes that generally underperform in terms of phase and group speed relative to their consistent-mass FEM/CVFEM counterparts.

Several of the finite difference and finite volume methods show reasonable dispersion characteristics, however it should be noted that, except for the first-order upwind scheme, these methods all involve higher-order advection operators, i.e. they involve more than just the neighbouring grid points. These methods are more difficult to deal with on unstructured meshes and many current implementations use extrapolation of variables outside the control volume

(e.g. Jessee and Fiveland [3]). The effect of this extrapolation on the resulting accuracy may be a concern and could be assessed using the methods outlined in this paper.

In terms of numerical performance for pure diffusion problems, the consistent mass CVFEM scheme introduces minimal error and anisotropy in two dimensions. In contrast, the stabilized schemes, FEM-SUPG and CVFEM-SUCV, may be optimized for phase and group accuracy, but when tuned for phase accuracy, they do not perform well in terms of the discrete diffusivity, which exhibits significant anisotropic behaviour. This reinforces the notion that there is no single best method that spans all problem classes.

4.2. Conclusions

The results of this *first step* in a multi-methods comparison lead us to conclude that:

- There is no *single* best method, but there are a number of competing methods that are of second-order accuracy or better and that should perform adequately in the hands of an experienced analyst. However, the grid resolution requirements to attain a certain level of error can be vastly different. The ultimate decision on a 'best' method for a given problem can be easily discerned by using the computational efficiency, i.e. CPU time, to achieve a given level of accuracy as a metric (see for example, Reference [4]).
- A single numerical method that can optimally solve all problem classes with equivalent accuracy and robustness does not exist in the set of methods considered, but the selection of an optimal numerical method must still be made based on the problem to be solved. The results presented here will hopefully provide some guidance in the selection process.
- The spatial coupling of time-derivatives yields super-convergent phase and group accuracy for the finite element methods, and as a general rule improves the phase and group accuracy of the CVFEM methods, albeit without the super-convergent behaviour.
- The two-dimensional dispersive properties of many of the methods may be characterized by a simple generalization relative to the corresponding one-dimensional behaviour.
- At the hyperbolic limit, the accurate propagation of a signal depends on providing adequate resolution for all wavelengths present in the signals. Dispersive errors will occur for all of the methods considered here.
- Although not often discussed, accurate modeling of diffusion also requires providing adequate resolution for all wavelengths present in the signals. Many methods exhibit reduced apparent diffusivities for short-wavelength signals, i.e. near the grid Nyquist limit.
- The artificial viscosity, in general, damps the under-resolved parts of a signal—the specific spectral characteristics have been shown to be a function of the method. All of the higher-order methods tend to introduce minimal artificial diffusivity through the mid-range of the discrete spectrum with a peak occurring just before the Nyquist limit for the grid. This behaviour may be optimized to deliver specific band-pass properties that match the dispersive properties of the method. However, to our knowledge, this type of matching has not been performed.

4.3. Future directions

The work presented here constitutes a first step in a multi-methods comparison intended to identify the relative strengths and weaknesses of multiple numerical methods in the context of

advective–diffusive processes. The focus for this work has been on characterizing the numerical artifacts associated with spatial discretization in a spectral sense. There are, of course, other numerical methods, and analysis techniques that can be applied to a multi-methods comparison. From our perspective the logical next steps in this work should proceed as follows.

1. Extend the analysis techniques presented here to treat non-linear advection methods. This step should consider the very important total-variation diminishing (TVD) properties of non-linear methods and the concomitant introduction of an artificial diffusivity that varies in space and time. Initial efforts in this direction suggest that it is possible to bound the phase and group speed, discrete diffusivity, and artificial diffusivity in terms of flux limiters and their operating range.
2. Extend the analysis presented here to consider the fully-discrete situation for a range of time-integration methods. Gresho and Sani [2] (see Section 2.7.6) present a prototypical study of fully discrete methods, albeit a subset of the methods considered here. In addition to characterizing the fully discrete dispersive errors, consideration of the algorithmic damping associated with time-integration schemes should be considered in conjunction with the artificial diffusivity associated with the spatial discretization. As with this work, a Fourier analysis would provide the means for placing all methods on a relatively equal footing.
3. A carefully designed suite of computational experiments should be assembled and used to assess specific methods selected based on the outcome of steps 1 and 2. This phase of the effort would focus on the development of an archival database of results that would be accessible via the world-wide web. This idea is not new, and a good prototype for this may be found in the work reported by Baptista *et al.* [5]. It is anticipated that this phase of the effort could draw on results provided by a large number of researchers with appropriate quality-control measures for submitted results.

ACKNOWLEDGEMENTS

The authors would like to acknowledge Tim Trucano and Tom Smith for their help during the development of this work, and for their helpful comments during the preparation of this paper. This work was supported under the ASCI Advanced Spatial Discretization project. Sandia is a multiprogram laboratory operated by Sandia Corporation, a Lockheed Martin Company for the United States Department of Energy's National Nuclear Security Administration under contract DE-AC04-94AL85000.

REFERENCES

1. Christon MA, Martinez MJ, Voth TE. Generalized fourier analysis of semi-discretizations of the advection–diffusion equation—Part I: one-dimensional domains. *International Journal for Numerical Methods in Fluids* 2004; **45**:839–887.
2. Gresho PM, Sani RL. Incompressible flow and the finite element method. *Advection–Diffusion and Isothermal Laminar Flow*. Wiley: Chichester, England, 1998.
3. Jessee JP, Fiveland WA, Howell LH, Colella P, Pember RB. An adaptive mesh refinement algorithm for the radiative transport problem. *Journal of Computational Physics* 1998; **139**:380–398.
4. Christon MA, Ketcheson DI, Robinson AC. An assessment of semi-discrete central schemes for hyperbolic conservation laws. SAND2003-3238, Sandia National Laboratories, Albuquerque, New Mexico, May 2003.
5. Baptista AM, Adams EE, Gresho P. Benchmarks for the transport equation: the convection–diffusion equation and beyond. *Quantitative Skill Assessment for Coastal Ocean Models* 1995; **47**:241–268.